PLOS PATHOGENS

RESEARCH ARTICLE

# Exploring the metabolic profile of *A. baumannii* for antimicrobial development using genome-scale modeling

**Nantia Leonidou**[1,2,3,4,5]*, **Yufan Xia**[2], **Lea Friedrich**[6], **Monika S. Schütz**[4,6], **Andreas Dräger**[1,4,5,7]

**1** Computational Systems Biology of Infections and Antimicrobial-Resistant Pathogens, Institute for Bioinformatics and Medical Informatics (IBMI), Eberhard Karl University of Tübingen, Tübingen, Germany, **2** Department of Computer Science, Eberhard Karl University of Tübingen, Tübingen, Germany, **3** Cluster of Excellence 'Controlling Microbes to Fight Infections', Eberhard Karl University of Tübingen, Tübingen, Germany, **4** German Center for Infection Research (DZIF), partner site Tübingen, Germany, **5** Quantitative Biology Center (QBiC), Eberhard Karl University of Tübingen, Tübingen, Germany, **6** Interfaculty Institute for Microbiology and Infection Medicine, Institute for Medical Microbiology and Hygiene, University Hospital Tübingen, Tübingen, Germany, **7** Data Analytics and Bioinformatics, Institute of Computer Science, Martin Luther University Halle-Wittenberg, Halle (Saale), Germany

* nantia.leonidou@uni-tuebingen.de





**Citation:** Leonidou N, Xia Y, Friedrich L, Schütz MS, Dräger A (2024) Exploring the metabolic profile of *A. baumannii* for antimicrobial development using genome-scale modeling. PLoS Pathog 20(9): e1012528. https://doi.org/10.1371/journal.ppat.1012528

**Editor:** Matthew Parsek, University of Washington, UNITED STATES OF AMERICA

**Received:** February 8, 2024

**Accepted:** August 26, 2024

**Published:** September 23, 2024



**Data Availability Statement:** The model *i*ACB23LX together with all curated and refined models are available at the BioModels Database (https://www.ebi.ac.uk/biomodels/) as SBML Level 3 Version 1 files. The following identifiers can be used to access the individual models: MODEL2406250010, MODEL2406250011, MODEL2406250005, MODEL2406250007, MODEL2406250008, MODEL2406250006, MODEL2406250009, and MODEL2309120001. All other relevant data are in the manuscript and its Supporting information files.

## Abstract

With the emergence of multidrug-resistant bacteria, the World Health Organization published a catalog of microorganisms urgently needing new antibiotics, with the carbapenem-resistant *Acinetobacter baumannii* designated as "critical". Such isolates, frequently detected in healthcare settings, pose a global pandemic threat. One way to facilitate a systemic view of bacterial metabolism and allow the development of new therapeutics is to apply constraint-based modeling. Here, we developed a versatile workflow to build high-quality and simulation-ready genome-scale metabolic models. We applied our workflow to create a metabolic model for *A. baumannii* and validated its predictive capabilities using experimental nutrient utilization and gene essentiality data. Our analysis showed that our model *i*ACB23LX could recapitulate cellular metabolic phenotypes observed during *in vitro* experiments, while positive biomass production rates were observed and experimentally validated in various growth media. We further defined a minimal set of compounds that increase *A. baumannii*'s cellular biomass and identified putative essential genes with no human counterparts, offering new candidates for future antimicrobial development. Finally, we assembled and curated the first collection of metabolic reconstructions for distinct *A. baumannii* strains and analyzed their growth characteristics. The presented models are in a standardized and well-curated format, enhancing their usability for multi-strain network reconstruction.

## Author summary

The emergence of multidrug-resistant bacteria, particularly carbapenem-resistant *Acinetobacter baumannii*, has become a severe global health threat. This pressing issue

**Funding:** This work was funded by the Deutsche Forschungsgemeinschaft (DFG, German Research Foundation) under Germany's Excellence Strategy – EXC 2124 – 390838134 to NL, and supported by the Cluster of Excellence 'Controlling Microbes to Fight Infections' (CMFI). N.L. and A.D. are supported by the German Center for Infection Research (DZIF, doi: 10.13039/100009139) within the Deutsche Zentren der Gesundheitsforschung (BMBF-DZG, German Centers for Health Research of the Federal Ministry of Education and Research, BMBF), grant No8020708703. The authors acknowledge the support by the Open Access Publishing Fund of the University of Tübingen (https://uni-tuebingen.de/en/216529) to NL. The funders had no role in study design, data collection and analysis, decision to publish, or preparation of the manuscript.

**Competing interests:** The authors have declared that no competing interests exist.

necessitated the development of new antibiotics, as highlighted by the World Health Organization. To address this need, we aimed to create comprehensive metabolic models to better understand bacterial metabolism and aid in developing novel therapeutic strategies. In this study, we developed a versatile workflow to construct high-quality, simulation-ready genome-scale metabolic models for bacterial pathogens. Applying this workflow, we constructed a metabolic model for *A. baumannii* and validated its accuracy using experimental data. The model successfully replicated observed metabolic phenotypes and identified essential genes without human counterparts, suggesting potential targets for new antibiotics. Additionally, we assembled and curated the first collection of metabolic reconstructions for distinct *A. baumannii* strains, analyzing their growth characteristics. These standardized and well-curated models enhance usability, facilitating multi-strain network reconstruction and further research. These findings provide a robust tool for understanding *A. baumannii*'s metabolism, guiding the development of new antimicrobial therapies.

## Introduction

In the 21st century, treating common bacterial infections has become a global health concern. The rapid emergence of pathogens with newly developed resistance mechanisms led to the ineffectiveness of hitherto used antimicrobial drugs. According to their resistance patterns, bacteria are classified into three main categories: multidrug-resistant (MDR, resistant to at least one agent in more than three antibiotic categories), extensively drug-resistant (XDR, non-susceptible to one or two categories), and pandrug-resistant (PDR, non-susceptible to all drugs in all categories) [1]. Pathogens from the last two classes are called "superbugs". In February 2022, Murray *et al.* developed predictive statistical models within a large-scale global study and estimated 1.27 million deaths directly associated with antimicrobial resistance (AMR) [2]. The same study underlines the highly virulent ESKAPE pathogens (*Enterococcus faecium*, *Staphylococcus aureus*, *Klebsiella pneumoniae*, *Acinetobacter baumannii*, *Pseudomonas aeruginosa*, and *Enterobacter* spp.) as the primary cause of AMR-related deaths, while the World Health Organization (WHO) announced in 2017 the urgent need for novel and effective therapeutic strategies against these microorganisms, assigning them the "critical status".

Over the years, numerous studies highlighted the Gram-negative human pathogen *Acinetobacter baumannii* of substantial concern in hospital environments attributable to its high intrinsic resistance against antimicrobial agents, including biocides [3–6]. *A. baumannii* (from the Greek word *akínētos*, meaning "unmoved") is a rod-shaped, non-motile, and strictly aerobic bacterium. It is an opportunistic pathogen whose adaptable genetic apparatus has caused it to become endemic in intensive care units (ICUs), affecting immunocompromised patients, causing pneumonia, bacteremia, endocarditis, and more. Especially the carbapenem-resistant *A. baumannii* poses a serious global threat with high mortality rates [7–9]. It targets exposed surfaces and mucous tissues, colonizes the human nose [10–12], and is frequently associated with Severe Acute Respiratory Syndrome Coronavirus 2 (SARS-CoV-2) infections [13–16]. The skin has shown to be a community reservoir for *A. baumannii* in a very small percentage of samples [17, 18], while its prevalence in the soil is a frequent misconception as species from the genus *Acinetobacter* are ubiquitous in nature [5, 19]. Finally, it shows susceptibility to commonly used drugs, like $\beta$-lactams, aminoglycosides, and polymyxins. The strain ATCC 17978 is a widely studied nosocomial strain notable for its fully sequenced genome that provides a comprehensive genetic framework for researchers. Historically, it was first isolated in 1951

from a 4-month-old infant with fatal meningitis [20]. Smith *et al*. sequenced its complete genome using high-density pyrosequencing [20]. They reported the presence of putative pathogenic islands with virulence genes, including a large island with transposons and integrases, as well as elements resembling the Legionella/Coxiella Type IV secretion system, crucial for pathogenesis. Moreover, it is a human-adapted isolate and was the first to be discovered with an active type VI secretion system (T6SS) encoded on its chromosome [21]. Another remarkable characteristic is its utilization of microcin Mcc17978 to combat other bacteria such as closely related *Acinetobacter* species and *E. coli* through contact and T6SS-independent competition activity [22]. Previous studies have noted ATCC 17978 for its susceptibility to clinically important antibiotics, serving as a valuable model for studying the basic biology of *A. baumannii*, antibiotic susceptibility, and the mechanisms by which resistance can develop [23–26]. Finally, its lower level of antibiotic resistance makes it valuable for studying the basic mechanisms of antibiotic action and resistance development, while it is easier to genetically manipulate [27].

Systems biology, and especially the field of genome-scale metabolic network analysis, is the key to exploring genotype-phenotype relationships, better understanding mechanisms of action of such threatening pathogens, and ultimately developing novel therapeutic strategies. Genome-scale metabolic models (GEMs) combined with constraint-based modeling (CBM) provide a well-established, fast, and inexpensive *in silico* framework to systematically assess an organism's cellular metabolic capabilities under varying conditions having only its annotated genomic sequence [28]. As of today, GEMs have numerous applications in metabolic engineering, contributing to the formulation of novel hypotheses towards the detection of new potential pharmacological targets [29].

It has been more than a decade since the release of the first mathematical model representing *A. baumannii*'s metabolism. Kim *et al*. integrated biological and literature data to manually build AbyMBEL891, representing the strain AYE [30]. This model was further employed as an essential foundation for future reconstructions; however, its non-standardized and missing identifiers limited its use. Following a tremendous increase in the volume of literature and experimental data on *A. baumannii* (over 5,670 articles published between 2010 and 2017 according to PubMed), two new strain-specific metabolic networks emerged: the *i*LP844 [31] and the AGORA (Assembly of Gut Organisms through Reconstruction and Analysis) model [32]. Both networks were reconstructed through a semi-automated process and simulated the metabolism of two distinct strains: ATCC 19606 and AB0057, respectively. With the help of transcriptomic data of sampled colistin responses and *i*LP844, it was observed that the type strain ATCC 19606 underwent metabolic reprogramming, demonstrating a stress condition as a resistance mechanism against colistin exposure. Alterations in gene essentiality phenotypes between treated and untreated conditions enabled the discovery of putative antimicrobial targets and biomarkers. Moreover, the model for AB0057 was part of an extensive resource of GEMs built to elucidate the impact of microbial communities on host metabolism. The amount of mass- and charge-balanced reactions in these models is very high; however, they carry few to no database references. Norsigian *et al*. improved and expanded AbyMBEL891 to finally create the high-quality model *i*CN718 with a prediction accuracy of over 80% in experimental data [33], while Zhu *et al*. built a GEM for ATCC 19606 (*i*ATCC19606) integrating multi-omics data [34]. Compared to *i*LP844, *i*ATCC19606 incorporates metabolomics data together with transcriptomic data enabling the deciphering of bactericidal activity upon polymyxin treatment and the interplay of various metabolic pathways. Last but not least, in 2020, the first *in vivo* study on *A. baumannii* infection was published utilizing constraint-based modeling [35]. This time, the collection of strain-specific models was enriched with the first GEM for the hyper-virulent strain AB5075 (*i*AB5075). The model was validated using various

experimental data, while transcriptomics data was leveraged to identify critical fluxes leading to mouse bloodstream infections. Our literature search revealed one additional metabolic model of *A. baumannii* ATCC 17978, named *i*JS784 [36]. As of the time of writing, this model has not been officially published in a scientific journal or been deposited in a mathematical models' database. Nonetheless, the model cannot produce biomass even when all uptake reactions are open and all medium nutrients are available to the cell, making it unusable and hampering reproducibility.

We expanded the collection of *A. baumannii* GEMs by building a high-quality model for the nosocomial strain ATCC 17978, named *i*ACB23LX. The presented model follows the FAIR data principles and community standards and recapitulates experimentally-derived phenotypes with high predictive capability and accuracy scores. We enriched the model with numerous database cross-references and inferred the minimal nutritional requirements computationally. Moreover, we used this model to investigate the organism's growth ability in defined media and a medium simulating human nasal secretions while we assessed its ability to predict essential genes using different optimization approaches. Among the examined strains, ATCC 17978 is one of the most well-studied, with a substantial amount of experimental data available that can be used to direct model refinement and validation. Besides that, we systematically refined and evaluated all pre-existing reconstructions' performance to finally create the first compendium of curated and standardized models for *A. baumannii*. With this, we aim to support further studies to give new insights into this pathogen and promote strain- and species-specific therapeutic approaches.

## Materials and methods

### Growth curves of *A. baumannii*

Growth curves for *A. baumannii* strains AB5075, ATCC 17978, ATCC 19606, and AYE were recorded in Luria-Bertani (LB), *i*MinMed supplemented with acetate as sole carbon source (0.2% weight per volume), and synthetic nasal medium (SNM) [97]. Overnight cultures of the strains grown in LB were harvested by centrifugation, and the cell pellet was washed once with 5 mL of phosphate buffered saline (PBS). Cells were then re-suspended in the medium used for the growth curves. The starting optical density $(OD)_{600nm}$ was adjusted to 0.1 and growth curves were recorded in 2 mL of medium for 12 h in triplicates using a Tecan infinite M200 PRO plate reader and 12-well plates covered with a plastic lid. Plates were incubated with linear shaking at 37˚C and the $OD_{600nm}$ was measured every 15 min. Growth rates were determined as the slope of the linear part of the curves plotting the natural logarithm of $OD_{600nm}$ against time.

### Metabolic network reconstruction workflow

Fig 1 illustrates the workflow developed to create the high-quality genome-scale metabolic network *i*ACB23LX, following the state-of-the-art protocol by Thiele *et al.* [28]. Our workflow consists of eight major steps starting from the extraction of an annotated genome until the model validation using experimental data. Modifications in the model structure, as well as the inclusion of cross-references to multiple functional databases, were done using the libSBML [46] library, while all simulations were conducted via the constraints-based reconstruction and analysis for Python (COBRApy)-0.22.1 suite [58] that includes functions commonly used for simulations.

The individual steps are described below in more detail with respect to the reconstruction of *i*ACB23LX.

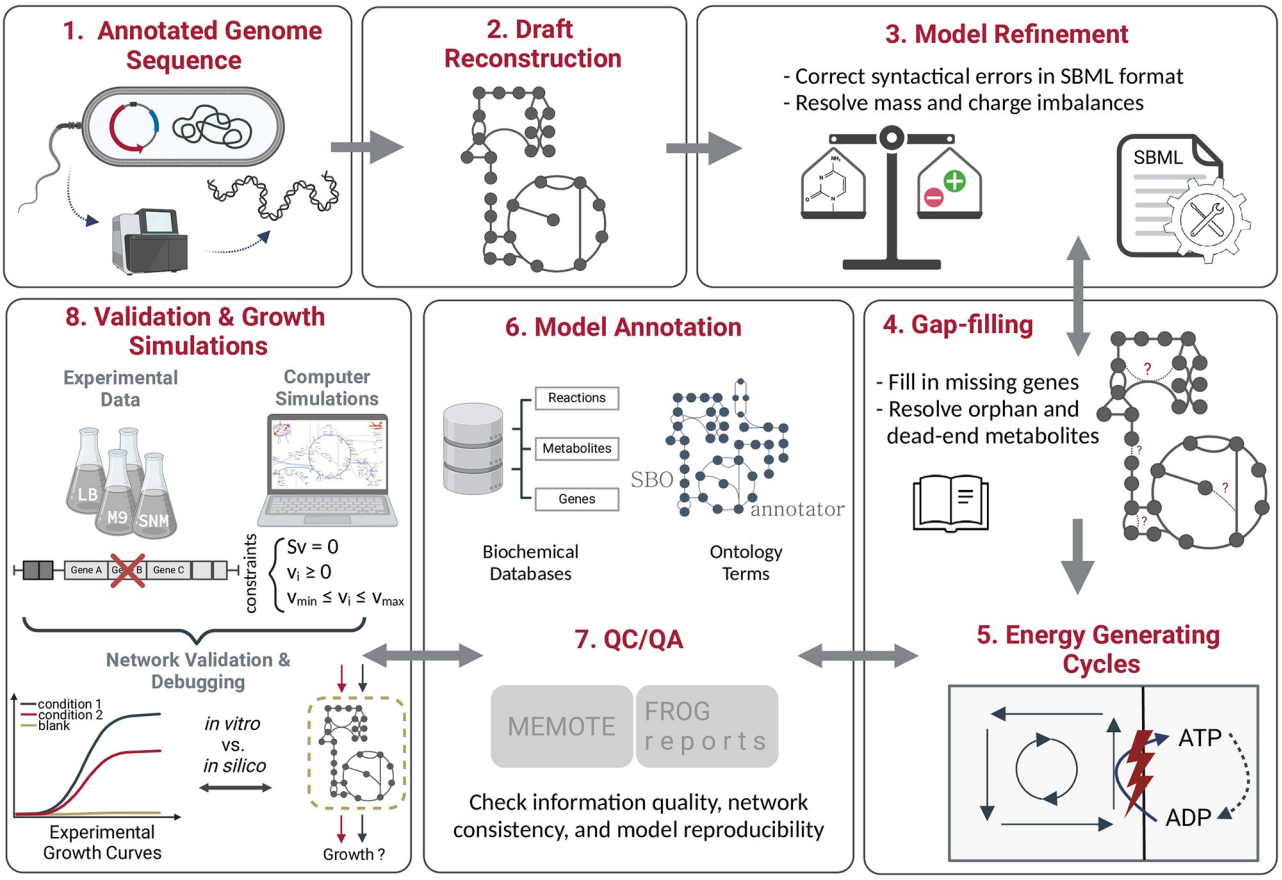


**Fig 1. Workflow developed for the metabolic network reconstruction of *i*ACB23LX.** The created workflow consists of eight main steps: extraction of the annotated genome, draft model reconstruction, model refinement, gap-filling, investigation of energy-generating cycles, model annotation, quality control and quality assurance (QC/QA), and model validation using experimental data. Growth simulations include the examination of growth requirements and the definition of a minimal growth medium. The last six processes are continuously iterated until the model reaches a satisfied quality and can recapitulate known phenotypes. Figure created with BioRender.com.

https://doi.org/10.1371/journal.ppat.1012528.g001

**Draft reconstruction.** The draft model was built with CarveMe version 1.5.1 using the annotated genome sequence of ATCC 17978 [39]. This was downloaded from the National Centre for Biotechnology Information (NCBI) at https://www.ncbi.nlm.nih.gov and has the assembly accession number `ASM1542v1` [20]. Seven strain-specific assemblies are registered in NCBI; however, the chosen entry is also registered in Kyoto Encyclopedia of Genes and Genomes (KEGG) [38], which supports the model extension. The genome is 3.9 Mbp long and has two plasmids (pAB1 and pAB2). We set the SBML flavor to activate the extension for flux balance constraints (fbc) version 2 [98]. This extension enables semantic descriptions for domain-specific elements, such as metabolite chemical formulas and charges, along with reaction boundaries and gene-protein-reaction associations (GPRs). Moreover, the optional parameter `gramneg` provided CarveMe was selected to employ the specialized template for the Gram-negative bacteria. Compared to the Gram-positive template, the Gram-negative template comes with phosphatidylethanolamines, murein, and a lipopolysaccharide unit. Its biomass reaction involves membrane and cell wall components resulting in more accurate gene essentiality predictions in the lipid biosynthesis pathways.

**Manual refinement and extension.** We started the manual refinement of the draft model by resolving syntactical errors within the Systems Biology Markup Language (SBML) [40]

model file using the SBML Validator from the libSBML [46]. These errors involve improper file structure, incorrect or missing tags, missing or improperly formatted attributes, and invalid values. Missing metabolite charges and chemical formulas were retrieved from the Biochemical, Genetical, and Genomical (BiGG) [70] and ChEBI [99] databases, while mass- and charge-imbalanced reactions were corrected. The most intense part of the workflow is the manual network extension and gap-filling. This was done using the organism-specific databases KEGG [38] and BioCyc [100], together with ModelSEED [71]. We mapped the new gene locus tags to the old ones using the GenBank General Feature Format (GFF) [101] and added missing metabolic genes along with the respective reactions and metabolites into our model. The network's connectivity was ensured by resolving as many dead-end (only produced but not consumed) and orphan (only consumed but not produced) metabolites as possible. Also, reactions with no connectivity were not included in the model, while reactions with no organism-specific gene evidence were removed from the model.

**Erroneous energy generating cycles.** Energy-generating cycles (EGCs) are thermodynamically infeasible loops found in metabolic networks and have not been experimentally observed, unlike futile cycles. EGCs charge energy metabolites such as adenosine triphosphate (ATP) and uridine triphosphate (UTP) without any external source of nutrients, which may lead to incorrect and unrealistic energy increases. Their elimination is crucial for correcting the energy metabolism, as they can inflate the maximal biomass yields and render unreliable predictions. We checked their existence in *i*ACB23LX applying an algorithm developed by Fritzemeier *et al.* [41].

We created a Python script that (1) defines and adds energy dissipation reactions (EDRs) in the network:

$$\mathrm{X[c]} + \mathrm{H_2O[c]} \longrightarrow \mathrm{X^+[c]} + \mathrm{H[c]} + \mathrm{Pi[c]},$$

where X is the metabolite of interest and (2) maximizes each EDR while blocking all influxes. This can be formulated as follows:

$$\max(v_{edr})$$

subject to

$$\begin{aligned} & S \cdot \vec{v} = 0 \\ & \forall i \notin E : v_i^{\min} \leq v_i \leq v_i^{\max} \\ & \forall i \in E : v_i = 0 \end{aligned} \tag{1}$$

where *edr* is the index of the current dissipation reaction, $S$ is the stoichiometric matrix, $\vec{v}$ the flux vector, $E$ the set of all exchange reactions, and $v_i^{\min}$ and $v_i^{\max}$ the upper and lower bounds. The existence of EGCs is indicated by a positive optimal value of $v_{edr}$.

Totally we examined 14 energy metabolites: ATP, cytidine triphosphate (CTP), guanosine triphosphate (GTP), UTP, inosine triphosphate (ITP), nicotinamide adenine dinucleotide (NADH), nicotinamide adenine dinucleotide phosphate (NADPH), flavin adenine dinucleotide (FADH2), flavin mononucleotide (FMNH2), ubiquinol-8, menaquinol-8, demethylmenaquinol-8, acetyl-coenzyme A (CoA), and L-glutamate. Moreover, we tested the proton exchange between cytosol and periplasm.

In the case of existing EGCs, we examined the directionality and the gene evidence of all participated reactions using organism-specific information from BioCyc as reference [100].

**Database annotations.** In this stage, the model was enriched with cross-linkings to various functional databases. Reactions and metabolites were annotated with relevant databases (e.g., KEGG [38], BRENDA [102], and UniProt [103]). These were included in the model as

controlled vocabulary (CV) Terms following the Minimal Information Required In the Annotation of Models (MIRIAM) guidelines [104] and the resolution service at https://identifiers.org/. We used ModelPolisher [105] to complete the missing available metadata for all metabolites and genes. Similarly, metabolic genes were annotated with their KEGG [38], NCBI Protein, and RefSeq identifiers using the GFF file [101]. Systems Biology Ontology (SBO) terms were assigned to different model entities using a freely accessible standalone tool called SBOannotator [43]. The SBO terms are structured controlled vocabularies used in computational modeling to define and describe model entities unambiguously [106]. The SBOannotator was developed to automatically assign precise SBO terms to SBML models, mainly focusing on biochemical reactions, thereby enhancing the reproducibility and usability of biochemical networks [43]. In addition, Evidence and Conclusion Ontology (ECO) terms were added to every reaction to capture the type of evidence of biological assertions with `BQB_IS_DESCRIBED_BY` as a biological qualifier. They are useful during quality control and mirror the curator's confidence about the inclusion of a reaction. When multiple genes encode a single reaction, an ECO term was added for every participant gene. Both terms were incorporated into the final model.

Finally, reactions were annotated with the associated subsystems in which they participate using the KEGG [38] database and the biological qualifier `BQB_OCCURS_IN`. Moreover, the "groups" plugin was activated [48]. Every reaction that appeared in a given pathway was added as a `groups:member`, while each pathway was created as a group instance with `sboTerm="SBO:0000633"` and `groups:kind="partonomy"`.

**Quality control and quality assurance.** The metabolic model testing (MEMOTE) [45] version 0.13.0 was used to assess and track the quality of our model after each modification, providing us with information regarding the model improvement. The Flux variability, Reaction deletion, Objective function, and Gene deletion (FROG) analysis framework was utilized to assess model reproducibility, ensuring reusability and results verification [47]. The resulting reports include comprehensive analyses of flux variability, reaction deletion, objective function, and gene deletion, providing a thorough evaluation of model performance. The final model was converted into the latest SBML Level 3 Version 2 [48] format using the libSBML package, while the SBML Validator tracked syntactical errors and ensured a valid format of the final model [46].

## Constraint-based analysis

The most frequently used constraint-based modeling approach is the flux balance analysis (FBA) that determines a flux distribution via optimization of the objective function and linear programming [59]. Prior to this, the metabolic network is mathematically encoded using the stoichiometric matrix *S* formalism. This structure delineates the connectivity of the network, and it is formed by the stoichiometric coefficients of all participating biochemical reactions. The rows and columns are represented by the metabolites and the mass- and charge-balanced reactions respectively. At steady state, the system of linear equations derived from the network is defined as follows:

$$\mathbf{S} \cdot \vec{v} = 0 \tag{2}$$

with **S** being the stoichiometric matrix and $\vec{v}$ the flux vector. With no defined constraints, the flux distribution may be determined at any point within the solution space. This space must be further restricted since the system is under-determined and algebraically insoluble. An allowable solution space is defined by a series of imposed constraints that are followed by cellular functions. Altogether the FBA optimization problem, with mass balance, thermodynamic, and

capacity constraints, is defined as:

$$\begin{aligned} &\text{max or min} && Z = c^T \vec{v} \\ &\text{subject to :} && \mathbf{S} \cdot \vec{v} = 0 \\ & && 0 \leq v_i \qquad \forall \text{ irreversible reactions } i \\ & && v_{\min} \leq v_i \leq v_{\max} \quad \text{for } i = 1, \ldots, n. \end{aligned} \tag{3}$$

Here, $n$ is the amount of reactions, $Z$ represents the linear objective function, and $\vec{c}$ is a vector of coefficients on the fluxes $\vec{v}$ used to define the objective function.

## Growth simulations

**Strict aerobic growth check.** At the time of writing, CarveMe does not include reconstruction templates to differentiate between aerobic and anaerobic species. The directionality of reactions that produce or consume oxygen may affect the model's ability to grow anaerobically. *A. baumannii* is defined to be a strictly aerobic species. Hence, we tested whether our model could grow with no oxygen supplementation. For this purpose, we examined all active oxygen-producing reactions under anaerobic conditions. We corrected their directionality based on the organism-specific information found in BioCyc [100] and kept only those with associated gene evidence.

**Defining a minimal growth medium.** To determine the minimal number of nutrients needed for the bacterium to grow, we defined a minimal medium using *i*ACB23LX. We determined the minimal amount of metabolites needed for growth using the M9 minimal medium (M9) (S1 Table) as a reference (*i*MinMed). We modeled growth on *i*MinMed by enabling the uptake of all metabolites that constitute the medium. The lower bound for the rest of the exchanges was set to 0 mmol/($g_{DW}$ · h). The final minimal medium is listed in Table 1 and in S1 Table. It consists of nine transition metals, a carbon source, a nitrogen source, a sulfur source, and a phosphorus source. The aerobic environment was simulated by setting the lower bound for the oxygen exchange to −10 mmol/($g_{DW}$ · h).

**Table 1. Composition of the computationally defined minimal growth medium, *i*MinMed.** It consists of nine transition metals, a carbon source, a nitrogen source, a sulfur source, and a phosphorus source. Oxygen was used to represent aerobic conditions.

| | Molecular Formula | Name |
|---|---|---|
| **Carbon source** | $C_2H_3O_2^-$ | Acetate |
| **Nitrogen source** | $NH_4^+$ | Ammonium |
| **Sulfur source** | $SO_4^{2-}$ | Sulfate |
| **Phosphorus source** | $HPO_4^{2-}$ | Phosphate |
| | $Ca^{2+}$ | Calcium |
| | $Cl^-$ | Chloride |
| | $Cu^{2+}$ | Copper |
| | $Fe^{3+}$ | Ferric iron |
| **Transition metals** | $Co^{2+}$ | Cobalt |
| | $K^+$ | Potassium |
| | $Mg^{2+}$ | Magnesium |
| | $Mn^{2+}$ | Manganese |
| | $Zn^{2+}$ | Zinc |
| **Oxygen source** | $O_2$ | Oxygen |

https://doi.org/10.1371/journal.ppat.1012528.t001

**Growth in chemically defined media.** We utilized experimentally verified growth media to examine the growth capabilities of *i*ACB23LX. The LB medium serves as a common medium for the cultivation of *A. baumannii*. Consequently, we conducted an assessment of our model's capacity to accurately simulate growth in this particular medium. Furthermore, we examined the growth of our model in the human nasal niche, considering that *A. baumannii* has been isolated from nasal samples within ICUs [10–12]. For this purpose, we utilized the SNM that imitates the human nasal habitat [97]. In all cases, if macromolecules or mixtures were present, we considered the constitutive molecular components for the medium definition. As our model was initially unable to reproduce growth on the applied media, we deployed the gap-filling option from CarveMe to detect missing reactions and gaps in the network [39]. All growth media formulations are available in S1 Table.

**Rich medium definition.** To investigate our model's growth rate when all nutrients are available to the bacterial cell, we defined the rich medium. For this purpose, we enabled the uptake of all extracellular metabolites by the model setting the lower bound of their exchange reactions to −10 mmol/($g_{DW}$ · h).

## Model validation

**Evaluation of carbon and nitrogen utilization.** We employed the previously published Biolog Phenotypic Array data by Farrugia *et al.* for *A. baumannii* ATCC 17978 to validate the functionality of our model [26]. According to the experimental guidelines provided by Farrugia *et al.*, we utilized M9 for all simulations [26]. The medium was then supplemented with D-xylose as a carbon source for the nitrogen testings, while ammonium served as the only nitrogen source for the carbon tests. As D-xylose was initially not part of the model, we conducted an extensive search in the organism-specific databases KEGG [38] and BioCyc [100] to include missing reactions.

The phenotypes were grouped by their maximal kinetic curve height. A trait was considered positive ("growth") if the height exceeded the 115 and 101 OmniLog units for a nitrogen and carbon source, respectively. The prediction accuracy was evaluated by comparing the *in silico*-derived phenotypes to the Biolog results. More specifically, the overall model's accuracy (ACC) was calculated by the overall agreement:

$$\mathrm{ACC} = \frac{TP + TN}{TP + TN + FP + FN} \tag{4}$$

where true positive (TP) and true negative (TN) are correct predictions, while false positive (FP) and false negative (FN) are inconsistent predictions. Discrepancies were resolved via iterative manual model curation.

**Gene perturbation analysis.** We performed *in silico* single-gene deletions on *i*ACB23LX to detect essential genes. For this purpose, we utilized the `single_gene_deletion` function from the COBRApy [58] package. A gene is considered to be essential if a flux of 0.0 mmol/($g_{DW}$ · h) is predicted through the biomass reaction after setting the lower and upper bounds of the associated reaction(s) to 0.0 mmol/($g_{DW}$ · h).

Additionally, we examined the effect of gene deletions using two different optimization approaches: FBA [59] and minimization of metabolic adjustment (MOMA) [60]. Contrary to FBA, MOMA is based on quadratic programming, and the involved optimization problem is the Euclidean distance minimization in flux space. Moreover, it approximates the metabolic phenotype and relaxes the assumption of optimal growth flux for gene deletions [60].

The results were compared to gene essentiality data [57]. Wang *et al.* generated a random mutagenesis dataset including 15,000 unique transposon mutants using insertion sequencing

(INSeq) [57]. Four additional transposon sequencing (Tn-seq) libraries of multiple *A. baumannii* isolates were employed to validate the model and increase confidence [57, 68, 77–79]. In this case only genes with an ortholog in `ASM1542v1` were considered. Analogously to the experimental settings, the nutrient uptake constraints were set to define the LB medium. From the 453 genes experimentally identified as essential, 191 could be compared to our predictions. The rest were not part of *i*ACB23LX due to their non-metabolic functions. To measure the effect of a single deletion, we calculated the fold change (FC) between the model's growth rate after ($gr_{KO}$) and before ($gr_{WT}$) a single knockout. This is formulated as follows:

$$FC_{gr} = \frac{gr_{KO}}{gr_{WT}} \tag{5}$$

To this end, if $FC_{gr} = 0$, the deleted gene is classified as essential, meaning its removal prevented the network from producing at least one key biomass metabolite predicting no growth. Similarly, if $FC_{gr} = 1$, the deletion of the gene from the network did not affect the growth phenotype (labeled as inessential), while when $0 < FC_{gr} < 1$, the removal of this gene affected partially the biomass production (labeled as partially essential). The complete lists of the gene essentiality results are available in S2 and S3 Tables.

To explore the potential of *in silico* identified essential genes as new drug candidates against *A. baumannii* infections, we probed the queries of predicted false negative candidates against the human proteome using Basic Local Alignment Search Tool (BLAST) [107]. The protein sequences were aligned to the human protein sequences using the default settings of the NCBI BLASTp tool (word size: 6, matrix: BLOSUM62, gap costs: 11 for existence and 1 for extension). To eliminate adverse effects and ensure no interference with human-like proteins, queries with any non-zero alignment score with the human proteome were not considered. Lastly, we searched the DrugBank database version 5.1.9 to find inhibitors or ligands known to act with the enzymes encoded by the non-homologous genes [66].

## Curation of existing metabolic networks

Previously reconstructed models of *A. baumannii* for multiple strains were collected and curated following community standards and guidelines. For this, we created a workflow that comprises four main steps and utilizes model validation and annotation tools. This can be applied to any metabolic network in SBML [40] format and follows the community "gold standards" strictly, as proposed by Carey *et al.* [37]. The curation steps involved changes in the format, amount, and quality of the included information. The context has not been altered in any way that could impact the models' prediction capabilities. We employed a combination of already existing tools to analyze, simulate, and quality-control the models (COBRApy [58], `MEMOTE` [45], and the SBML Validator [46]). Different database cross-references were incorporated in the models using ModelPolisher [105] and following the MIRIAM guidelines [104], while the libSBML library [46] was used to manipulate the file format and convert to the latest version. To resolve inflated growth rates, we determined computationally-defined minimal growth media. The growth capabilities were examined with respect to various experimentally-derived growth media, while the LB medium was applied to identify lethal genes. A strain-wise comparison was not feasible due to strain-specific identifiers, no successful growth, or missing genes. Hence, we investigated the essential genes across all models with identifiers that could be mapped with the Pathosystems Resource Integration Center (PATRIC) ID mapping tool [108].

To begin with the debugging, we examined the syntactical correctness and internal consistency of the downloaded files using the SBML Validator from the libSBML library [46]. Two models (*i*CN718 and *i*JS784) could not pass the validator check and reported errors since they

were not in a valid SBML [40] format right after their attainment. We made *i*CN718 valid by deleting the reaction `DNADRAIN` for which neither a reactant nor a product was assigned since the associated metabolite was not part of the model. Similarly, the empty `groups` attribute was removed from *i*JS784, converting the file into a valid format. Warnings were detected for *i*ATCC19606, and *i*AB5075 due to missing definition of the fbc extension (available at the latest Level 3 release [98]) and the non-alphanumeric chemical formulas. We resolved these issues by defining the fbc list `listOfGeneProducts` and the species attribute `chemicalFormula`. In more detail, we extracted the given GPRs from the notes field and defined individual `geneProduct` classes with `id`, `name`, and `label`. The attribute `chemicalFormula` was set equal to the species chemical formulas extracted from the notes and is particularly essential in reaction's validation and balancing. Following the SBML [40] specifications regarding its constitution, in case of ambiguous formulas separated by a semicolon (`;`), the first molecular representation was chosen. With this, the genes and metabolites' chemical formulas became part of the file's main structure. Since *i*ATCC19606 carried KEGG [38] identifiers, we could extract the metabolites' chemical formulas from the database and add them to the model. Moving on with the file extension, we declared the remaining missing attributes from reactions, metabolites, and genes that are required according to the SBML [40] language guidelines. More specifically, we defined the `metaid` attribute when missing, while we fixed any errors regarding the identifiers nomenclature. Further extension involved the annotation of reactions, metabolites, and genes with a plethora of database cross-references following the MIRIAM guidelines [104]. For this, we employed ModelPolisher that complements and annotates SBML [40] models with additional metadata using the BiGG Models knowledgebase as reference [105]. We also defined precise SBO terms with the `sboTerm` attribute using the SBOannotator [43]. The final step of debugging involved the conversion of all models to the newest available format SBML Level 3 Version 2 [48], as well as the quality control using `MEMOTE` [45].

## Results

### Reconstruction process of the metabolic network *i*ACB23LX

To build a high-quality model for *A. baumannii* ATCC 17978, we developed a workflow, as depicted in Fig 1, adhering closely to the community standards [37] (see Materials and methods).

We named the newly reconstructed network *i*ACB23LX, where *i* stands for *in silico*, ACB is the organism- and strain-specific three-letter code from the KEGG [38] database, 23 the year of reconstruction, and LX the modellers' initials. Our protocol involves eight major stages starting from the attainment of the annotated genomic sequence until the model validation, applies to any organism from the tree of life (Archaea, Bacteria, and Eukarya), and ensures the good quality and correctness of the final model. CarveMe [39] was used to build a preliminary model, which was subsequently extended and curated manually. We resolved SBML [40] syntactical issues and mass and charge imbalances during manual refinement while we defined missing metabolite charges and chemical formulas. Our final model contains no mass-imbalanced reactions and only two charge-imbalanced reactions. After extensive efforts, resolving all charge imbalances was impossible since all participated metabolites are interconnected to multiple reactions within the network. Hence, any modification in their charge resulted in newly introduced imbalances. The model extension process involved incorporating missing metabolic genes considering the network's connectivity. Dead-end and orphan metabolites do not exist biologically in the species, implying knowledge gaps in metabolic networks. Moreover, reactions including such metabolites are not evaluated in FBA. Therefore, reactions with

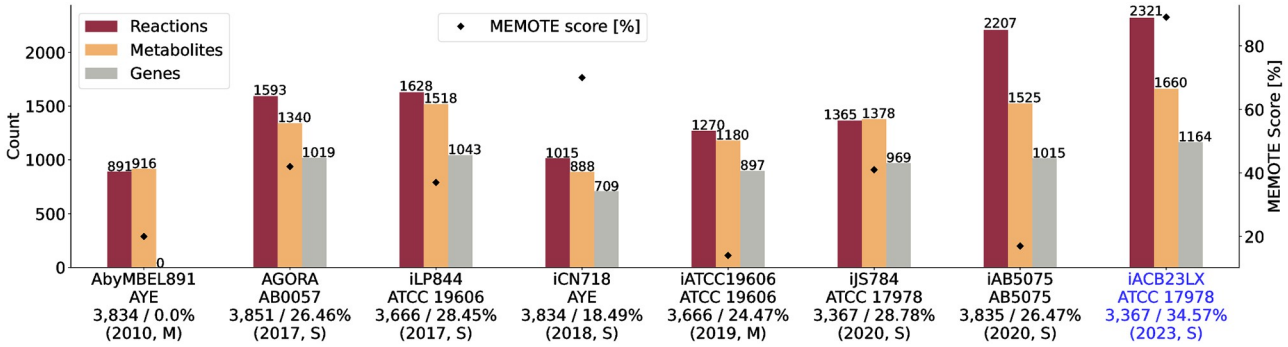


**Fig 2. Properties of all metabolic networks for *A. baumannii*.** Blue highlights the metabolic network for ATCC 17978 presented in this publication. The left ordinate shows the counts, while the right ordinate represents the MEMOTE scores. The abscissa labels are annotated with the respective strains, each accompanied by the count of open reading frames (ORFs) and the percentage of model gene coverage. The reconstruction process is divided into manual (M, nocomputational tool was used to reconstruct and refine the model) and semi-automated (S, draft obtained via an automated reconstruction tool, while further extension was done manually) and is written together with the publication year. The new model presented in this work exhibits the highest quality score and is more comprehensive and complete than the preceding reconstructions.

https://doi.org/10.1371/journal.ppat.1012528.g002

zero connectivity and no organism-specific gene evidence were omitted from the gap-filling. We extended the draft model by 138 reactions, 77 genes, and 110 metabolites in three compartments (cytosol, periplasm, and extracellular space). All in all, *i*ACB23LX comprises 2,321 reactions, 1,660 metabolites, and 1,164 genes (Fig 2). It is the most comprehensive model, while its stoichiometric consistency lies at 100% and contains no unconserved metabolites. Over 1,800 reactions have a GPR assigned, while 149 are catalysed by enzyme complexes (GPR contains at least two genes connected via a logical AND).

Furthermore, we tested our model for EGCs to prevent having thermodynamically infeasible internal loops that bias the final predictions [41]. We defined energy dissipation reactions (EDRs) for 15 energy metabolites, enabling transmission of cellular energy. Each reaction was individually added to the model and set as the objective function, while all uptakes were constrained to zero (see Materials and methods). A non-zero optimization result indicated an energy-generating cycle, which was then removed. With this, our final model, *i*ACB23LX, contains no EGCs. As shown in Fig 1, a plethora of database cross-references was embedded in the model, while SBO terms were defined for every reaction, metabolite, and gene [43]. Additionally, each reaction was mapped to an ECO term representing the confidence level and the assertion method (Fig 3).

To assess the model's quality, we utilized the Metabolic Model Testing tool (`MEMOTE`) [45] and the SBML [40] Validator from the libSBML library [46]. Our metabolic network, *i*ACB23LX, achieved a `MEMOTE` score of 89% with all syntactical errors resolved. Our model undoubtedly exhibits the highest quality score among its predecessors (Fig 2). Notably, the `MEMOTE` testing algorithm considers only the parent nodes of the SBO directed acyclic graph and not their respective children. Assigning more representative SBO terms does not increase the final score but reduces it by 2%. Finally, we assessed the model's reproducibility using FROG analyses [47] and submitted the reports along with our model to enable verification of results. The final model is available in SBML Level 3 Version 2 [48] and JavaScript Object Notation (JSON) formats with the fbc and groups plugins available.

## *i*ACB23LX is of high quality and exhibits an increased predictive accuracy

**Prediction and experimental validation of bacterial growth on various nutritional environments.** Constraint-based modeling approaches, such as FBA, estimate flux rates

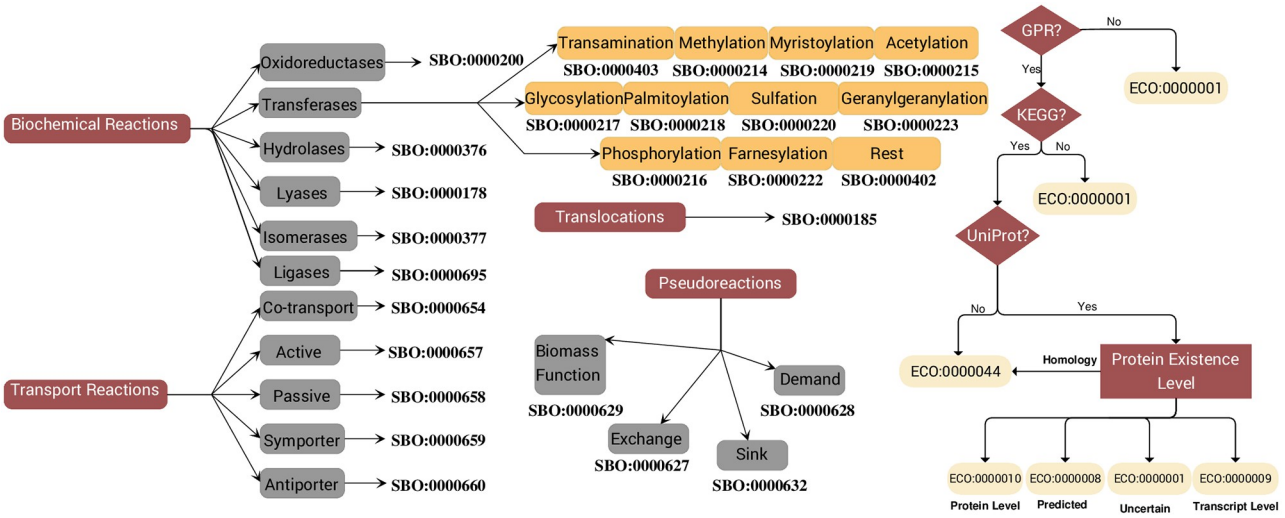


**Fig 3. Schematic representation of the SBO and ECO terms mapping.** It follows the graphs defined in the repository for biomedical ontologies Ontology Lookup Service (OLS) [42]. The SBO terms were added using the SBOannotator tool [43]. The ECO terms annotated metabolic reactions and were declared based on the presence of GPR along with KEGG and UniProt annotations. Providing UniProt identifiers, the Protein Existence Level guides the mapping to appropriate ECO terms. Figure created with yEd [44].

https://doi.org/10.1371/journal.ppat.1012528.g003

indicating how metabolites flow through the metabolic network and predict cellular phenotypes for various growth scenarios. *A. baumannii* is known to be strictly aerobic and, compared to the majority of *Acinetobacter* species, it is not considered ubiquitous in nature. As a nosocomial pathogen, it has been mostly detected in hospital environments, particularly in the ICUs, and within the human nasal microbiota [10–12]. We examined various growth conditions to ensure that *i*ACB23LX recapitulates these already known and fundamental phenotypes.

First, we tested our model's capability to simulate a strictly aerobic growth. For this purpose, we examined the directionality of all active oxygen-producing and -consuming reactions when the oxygen uptake was disabled (see S1 Fig). We observed an accumulation of periplasmic oxygen by reactions that carried remarkably high fluxes, leading to growth even when oxygen import was turned off. We examined each reaction individually and removed those without gene evidence to correct this. More specifically, we removed the periplasmic catalase (`CATpp`), one of bacteria's main hydrogen peroxide scavengers. This enzyme is typically active in the cytosol [49] and was not part of any precursor *A. baumannii* GEM or was found only in cytosol (*i*LP844 [31]). To fill the gap and enable the usage of the periplasmic hydrogen peroxide, we added the (`PEAMNOpp`) in the model. Eventually, *i*ACB23LX demonstrated growth only in the presence of oxygen using a rich medium (all exchange reactions are open).

Furthermore, we determined the minimal number of metabolites necessary for growth using *i*ACB23LX and the M9 as a reference. Minimal growth media typically consist of carbon, nitrogen, phosphorus, and sulfur sources, as well multiple inorganic salts and transition metals. These metals are crucial for the growth and survival of all three domains of life; however, they can be transformed into toxic compounds in hyper-availability [50]. The exact composition of our minimal medium (*i*MinMed) is shown in Table 1. It comprises nine transition metals, acetate as the carbon source, ammonium as a nitrogen source, sulfate as a sulfur source, and phosphate as a phosphorus source. Previous studies have highlighted the importance of nutrient metals for *A. baumannii* to survive within the host. More specifically, the bacterium utilizes these metals as co-factors for vital cellular processes [51]. Manganese and zinc have

**Table 2. Simulated and empirical growth rates of ATCC 17978 in various growth media.** The tested media are the computationally-defined minimal medium (*i*MinMed), the LB, and the SNM. Computational growth rates are given in mmol/($g_{DW}$ · h), while *in vitro* rates in $h^{-1}$. Doubling times are calculated in minutes. The media formulations are available in S1 Table.

| | Growth Rates | | Doubling Times | |
|---|---|---|---|---|
| | ***in silico*** | ***in vitro*** | ***in silico*** | ***in vitro*** |
| *i*MinMed | 0.5503 | 0.5402 | 75.57 | 76.70 |
| LB | 0.6065 | 0.7369 | 68.57 | 56.44 |
| SNM | 0.2914 | 0.3592 | 142.72 | 115.78 |

https://doi.org/10.1371/journal.ppat.1012528.t002

also been studied as essential determinants of host defense against *A. baumannii*-acquired pneumonia through their sequestering by calprotectin via a type of bonding called chelation [52]. In the computational simulations, growth rates below 2.81 mmol/($g_{DW}$ · h) were considered realistic. This threshold corresponds to the doubling time of the fastest-growing organism, *Vibrio natriegens*, which is 14.8 minutes [45]. Table 2 displays the predicted growth rates of *i*ACB23LX in the respective culture media. In LB, our model simulated with the highest growth rate; 0.6065 mmol/($g_{DW}$ · h). With our self-defined minimal medium, *i*MinMed, our model exhibited the lowest rate; 0.5503 mmol/($g_{DW}$ · h). Notably, our experimental validation revealed similarity between the growth rates obtained from the *in vitro* respiratory curves (Table 2 and S2 Fig) and those predicted by our *in silico* simulations. Additionally, we examined the growth rate of our model in a rich medium, in which all nutrients were available to the model. With this, the flux through the biomass production was the highest, 2.1858 mmol/($g_{DW}$ · h), as expected. This is still less than the growth rate of the fastest organism, increasing the confidence in our model's consistency and simulation capabilities. Initially, *i*ACB23LX could not predict any realistic growth rate for the simulated media. Using the gap-filling function of CarveMe [39], we detected three enzymes (`PHPYROX`, `OXADC`, and `LCYSTAT`) whose addition into the metabolic network resulted in successful growth in all tested media.

**Functional validation of *i*ACB23LX using nutrient utilization data.** Multiple *in silico* approaches have hitherto been employed to predict lethal genes and to assess growth metrics on different carbon/nitrogen sources for severe pathogenic organisms including *Mycobacterium tuberculosis* [53, 54] and *Staphylococcus aureus* [55, 56]. In 2013 and 2014, two studies were published that examined the catabolic phenome and gene essentialities of the strain ATCC 17978 [26, 57]. We used these datasets to evaluate the overall performance (functionality and accuracy) of *i*ACB23LX.

Our first validation experiment assessed the accuracy of our model's carbon and nitrogen catabolism potentials using the large-scale phenotypic data provided by Farrugia *et al.* [26]. While the authors tested a larger number of compounds overall, we were only able to examine 80 carbon sources and 48 nitrogen sources. For the remaining molecules, either no BiGG identifier existed, or they were not part of the metabolic network. Following the experimental protocol by Farrugia *et al*., we applied the M9 medium and enabled D-xylose as the sole carbon source for the nitrogen testings. As D-xylose was initially not part of the reconstructed network, we conducted extensive literature and database search to include associated missing reactions. This improved the prediction accuracy, especially for the carbon sources, where an amelioration of 19% was achieved. In more detail, despite the comprehensive manual curation, the first draft model was reconstructed using the automated tool CarveMe [39]. This resulted in the incorrect inclusion of transport reactions, which were consequently removed to reduce the number of false positive predictions. In both cases, our main objective was to improve the accuracy while keeping the number of orphan and dead-end metabolites low and removing

only reactions with no gene evidence (lack of assigned GPR). Similarly, missing reactions were identified and included in the network to eliminate the false negative predictions. For instance, in accordance with the phenotypic data, ATCC 17978 should not be able to grow when utilizing D-trehalose as the sole carbon source. Our model initially predicted a growth phenotype for this carbon source. To overcome this conflict, we deleted the reaction TREP with no organism-specific gene evidence, i.e., no assigned GPR. However, it was not feasible to resolve all inconsistencies since adding transport reactions to resolve false positives or false negatives in the nitrogen testings led to more false predictions in the carbon sources. More specifically, when adenosine, inosine, L-homoserine, and uridine are utilized as sole carbon sources, the model should not predict growth, while as sole nitrogen sources they should result in a non-zero objective value. In this case, adding transporters would resolve false predictions in the nitrogen tests, while it would have induced more false predictions in the carbon sources tests. Altogether, *i*ACB23LX exhibited an overall accuracy of 86.3% for the carbon and 79.2% for the nitrogen sources test (Fig 4c). By adding their corresponding transport reactions, we resolved discrepancies regarding uridine, inosine, adenosine, and L-homoserine. Our model was able to catabolize 49 sole carbon and 40 sole nitrogen sources (see Fig 4a and 4b), recapitulating totally 69 and 38 experimentally-derived phenotypes, respectively.

We further assessed the ability of *i*ACB23LX to predict known gene essentialities. First, 1,164 *in silico* single gene deletions were conducted on both LB and rich growth media, respectively to identify all lethal gene deletions. Subsequently, the ratio between the growth rate after and before the respective knockouts ($FC_{gr}$) was calculated, and the genes were classified accordingly (see Materials and methods). For the optimization, two mathematics-based approaches from the COBRApy [58] package were deployed: the FBA [59] and the MOMA [60]. Between the two methods, a similar distribution of the $FC_{gr}$ values was observed (Fig 5a and 5b). Using FBA, 97, 75, and 991 genes were predicted to be essential, partially essential, and inessential on LB, respectively. Similarly, optimization with MOMA resulted in 110, 85, and 968 genes (Fig 5c and S3 and S2 and S3 Tables). These genes were primarily associated with the biosynthesis of cofactors and vitamins, the amino acid/nucleotide metabolism, the energy metabolism, and the metabolism of terpenoids and polyketides. Additionally, we examined in more detail how nutrition availability impacts the gene essentiality by conducting single-gene knockouts in the rich medium. Both optimization methods yielded a higher number of essential genes when the model had to adapt its metabolic behavior due to lacking nutrients, i.e., with LB, compared to the rich medium (Fig 5c and S2 and S3 Tables). In general, FBA detected more genes to be dispensable for growth in both nutritional environments. On the other hand, MOMA classified more genes as essential or partially essential (Fig 5c and S2 and S3 Tables), while genes from FBA build a subset of the essential genes derived by MOMA. Furthermore, we validated the prediction accuracy of *i*ACB23LX using gene essentiality data. First, we analyzed the transposon mutant library developed by Wang *et al.* as it examines the same *A. baumannii* genome that we used to build our model [57].

Using this dataset and the LB medium, our model demonstrated a prediciton accuracy of 87% with both optimization methods (Fig 5d). To enhance the robustness and generalizability of our model across diverse datasets, we compared our model's predictions to four additional Tn-seq datasets. A total of 43 genes were labeled as essential in all studied Tn-seq data and were predicted as essential by our model. The derived predictive accuracies ranged between 86.6% and 88.9% (Fig 5e), underscoring the efficacy of our model across diverse high-throughput gene essentiality datasets. We further analyzed the predicted false negative genes and probed their proteomes to investigate the existence of human homologs (see Materials and methods and S4 Table). Our aim was to remove cross-linkings to human-similar proteins, as pathways or enzymes absent in humans are valuable sources of druggable targets against

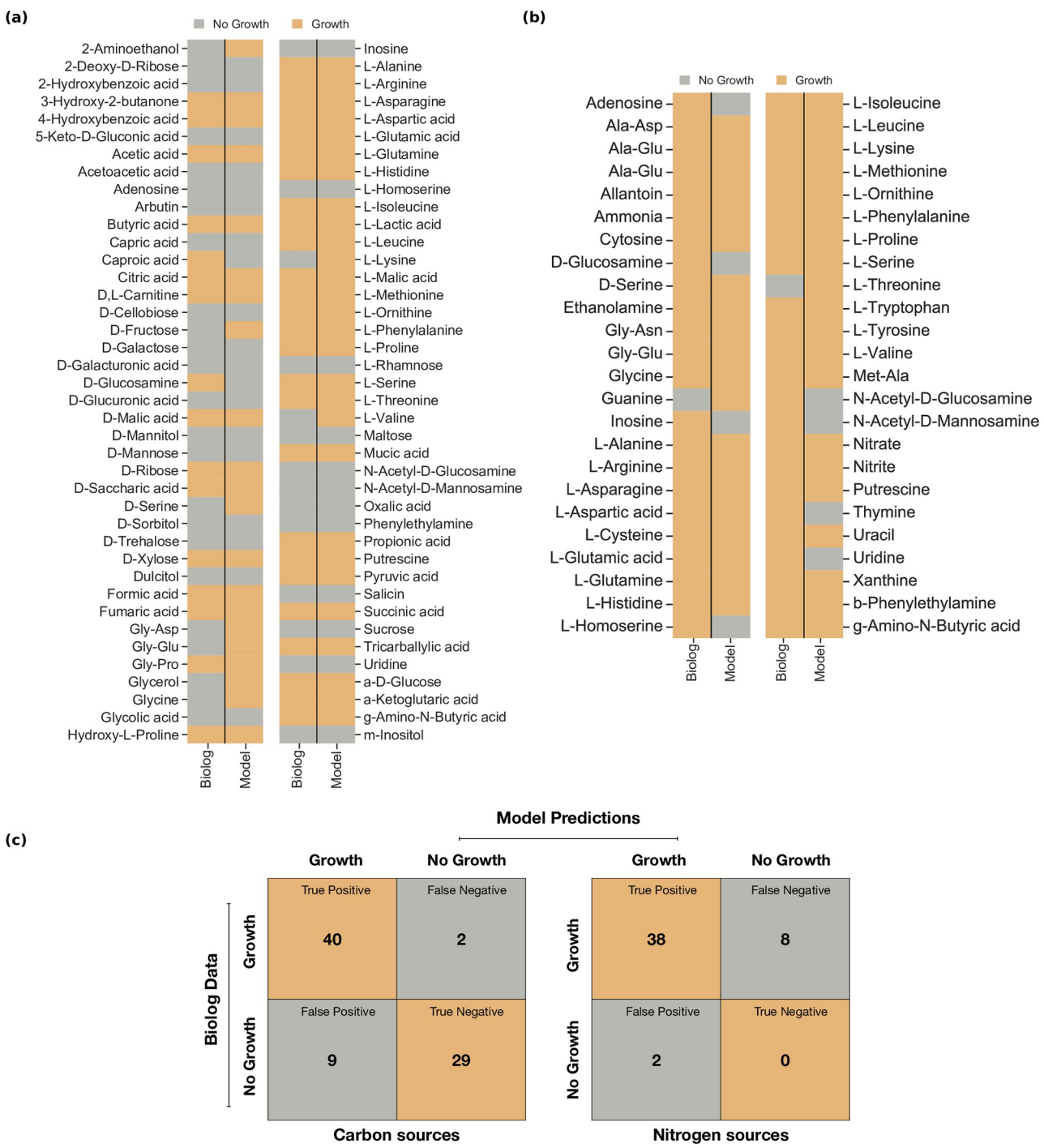


**Fig 4. Model predictions compared to the Biolog experimental measurements for various carbon and nitrogen sources.** From the Biolog data, only substances mappable to model metabolites were included, while the M9 medium was applied. **(a)** and **(b)** The model's ability to catabolize various carbon and nitrogen sources was assessed using the strain-specific phenotypic data by Farrugia *et al.* [26]. Grey indicates no growth, and orange indicates growth. Totally, 80 and 48 compounds were tested as sole carbon and nitrogen sources, respectively. Out of these, 69 and 38 phenotypes were recapitulated successfully by *i*ACB23LX. **(c)** Confusion matrices of model predictions and Biolog experimental measurements. The overall accuracy of *i*ACB23LX is 86.3% for the carbon (left matrix) and 79.2% for the nitrogen (right matrix) testings. Orange represents correct predictions, and grey represents wrong predictions.

https://doi.org/10.1371/journal.ppat.1012528.g004

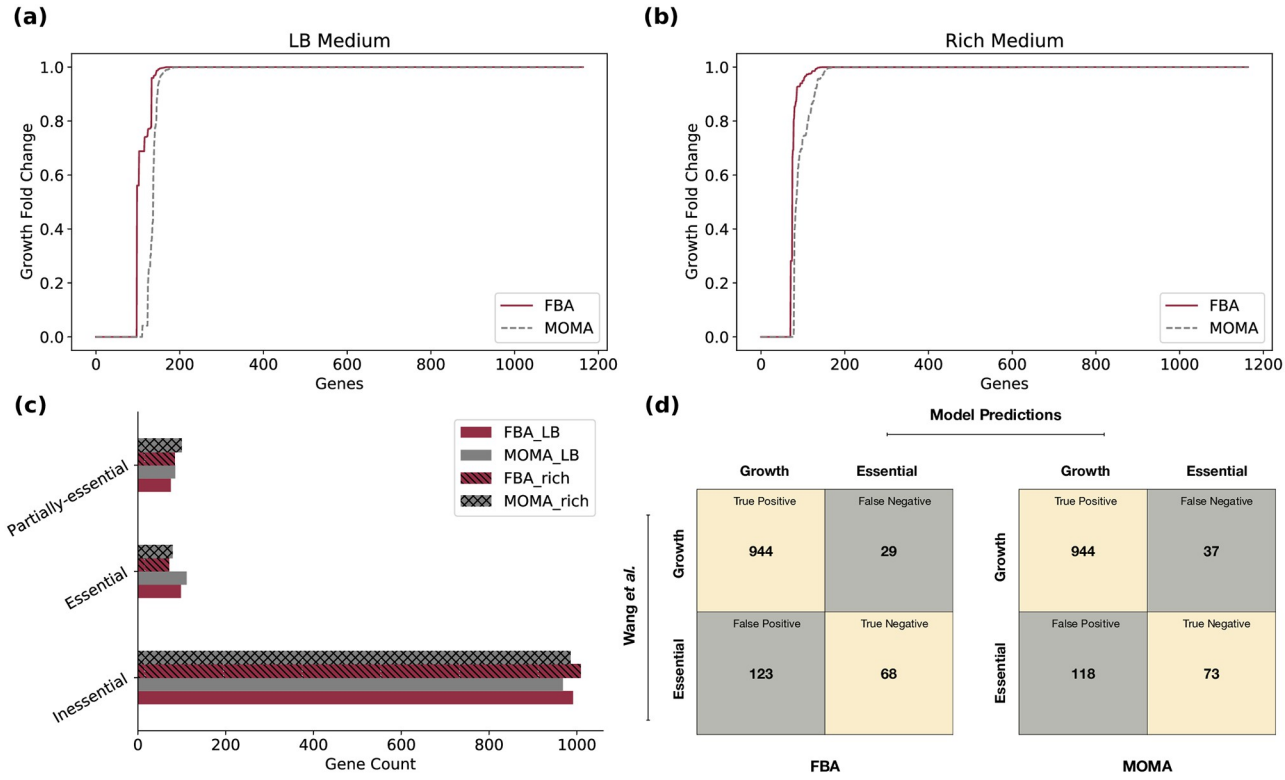


**(e)**

**FBA**

| | TP | FN | FP | TN | ACC |
|---|---|---|---|---|---|
| Gallagher *et al.* (2015) | 960 | 26 | 107 | 71 | 88.57% |
| Geisinger *et al.* (2020) | 960 | 39 | 107 | 58 | 87.46% |
| Bai *et al.* (2021) | 952 | 38 | 115 | 59 | 86.86% |
| Bai *et al.* (2023) | 972 | 34 | 95 | 63 | 88.92% |

**MOMA**

| | TP | FN | FP | TN | ACC |
|---|---|---|---|---|---|
| Gallagher *et al.* (2015) | 952 | 34 | 102 | 76 | 88.32% |
| Geisinger *et al.* (2020) | 952 | 47 | 102 | 63 | 87.20% |
| Bai *et al.* (2021) | 944 | 46 | 110 | 64 | 86.60% |
| Bai *et al.* (2023) | 964 | 42 | 90 | 68 | 88.66% |

**Fig 5. Gene essentiality analysis using *i*ACB23LX. (a)** and **(b)** Distribution of the $FC_{gr}$ values calculated for all genes included in *i*ACB23LX. Red lines represent FBA predictions and grey are ratios derived with MOMA. Totally 1,164 knockouts were conducted using each method in LB and rich media. **(c)** Classification of gene essentialities in essential, inessential, and partially essential based on their $FC_{gr}$ values. **(d)** Accuracy of gene essentiality predictions based on empirical data. The *in silico* results were compared to the Wang *et al.* transposon library [57]. The LB medium was applied to mirror the experimental settings. The metabolic network exhibited 87% accuracy with FBA (left) and MOMA (right). Beige indicates correct predictions; grey indicates incorrect predictions. **(e)** Comparative analysis of essential genes predicted by *i*ACB23LX versus those identified in multiple Tn-seq studies.

https://doi.org/10.1371/journal.ppat.1012528.g005

infectious diseases [61]. Out of the 37 genes that our model predicted to be essential using FBA and MOMA, which contradicted the experimental results, 17 were found to be non-homologous to human (S4 Table). Genes with a zero similarity score were defined as non-homologous, while those with a non-zero similarity score were excluded to avoid targeting human-

like proteins. Some examples are the genes encoding the enolpyruvylshikimate phosphate (EPSP) synthase (A1S_2276), chorismate synthase (A1S_1694), riboflavin synthase (A1S_0223), phosphogluconate dehydratase (A1S_0483), dihydrofolate reductase (DHFR) (A1S_0457), and 2-keto-3-deoxy-6-phosphogluconate (KDPG) aldolase (A1S 0484). The EPSP synthase converts the shikimate-3-phosphate together with phosphoenolpyruvate to 5-O-(1-carboxyvinyl)-3-phosphoshikimic acid. Subsequently, the chorismate synthase catalyses the conversion of the 5-O-(1-carboxyvinyl)-3-phosphoshikimic acid to chorismate, the seventh and last step within the shikimate pathway [62]. Chorismate is the common precursor in the production of the aromatic compounds tryptophan, phenylalanine, and tyrosine, as well as folate and menaquinones during the bacterial life cycle. The shikimate pathway is of particular interest due to its absence from the human host metabolome and its vital role in bacterial metabolism and virulence. Moreover, the enzyme riboflavin synthase catalyses the final step of riboflavin (vitamin B2) biosynthesis with no participating cofactors. Riboflavin can be produced by most microorganisms compared to humans, who have to externally uptake them via food supplements. Also, it plays an important role in the growth of different microbes, especially due to its photosynthesizing property that marks it as a non-invasive and safe therapeutic strategy against bacterial infections [63]. Lastly, the phosphogluconate dehydratase catalyses the dehydration of 6-phospho-D-gluconate to KDPG, the precursor of pyruvate and 3-phospho-D-glycerate [64]. This enzyme is part of the Entner–Doudoroff pathway that catabolizes glucose to pyruvate, similarly to glycolysis, but using a different set of enzymes [65].

We further assessed the druggability of our essential non-homologous proteins and investigated the existence of inhibitors or compounds known to interact with the enzymes. For this, we used the online DrugBank database that contains detailed information on various drugs and drug targets [66]. In all cases, the listed drugs are of unknown pharmacological action, and there is still no evidence indicating the enzymes' association with the molecule's mechanism of action. For instance, the flavin mononucleotide and the cobalt hexamine ion were listed as known inhibitors of yet unknown function against the chorismate synthase, while glyphosate, shikimate-3-phosphate, and formic acid have been experimentally found to act with EPSP synthase. Six non-homologous genes were marked as hypothetical or putative in the KEGG [38] database and/or lacked enzyme-associated information. We searched for drug leads by aligning the query sequences against the DrugBank's database to find homologous proteins. Two out of six were found to have a protein hit. More specifically, the protein encoded by A1S_0589 was found to have high sequence identity with the phosphocarrier protein HPr of *Enterococcus faecalis* (Bit-score: 48.5), while the translation product of A1S_0706 resembles the sugar phosphatase YbiV of *Escherichia coli* (Bit-score: 225.3). According to DrugBank, dexfosfoserine and aspartate beryllium trifluoride have been experimentally determined to bind to these enzymes; however, their pharmacological action is still unknown. The S4 Table lists all non-homologous essential genes reported for *i*ACB23LX.

Overall, *i*ACB23LX exhibits high agreement to all validation tests and can, therefore, be used to systematically derive associations between genotypes and phenotypes.

## A curated collection of *A. baumannii* metabolic models

In 2010, Kim *et al.* published the first GEM for the multidrug-resistant strain *A. baumannii* AYE [30]. After that, multiple studies provided new data and genomic analyses were published, paving new ways towards its update and refinement [26, 57, 67, 68]. Since then, a variety of GEMs was developed aiming at the empowering of drug development strategies and the enforcement of metabolic engineering by formulating new and reliable hypotheses (Table 3). However, the amount and format of information contained are inconsistent, with some being

**Table 3. List of genome-scale metabolic models curated for *A. baumannii*, along with information relevant to the manual refinement.** Default growth rates (i.e., model simulated as downloaded), the cellular compartments (C: cytosol, E: extracellular space, P: periplasm, and ER: endoplasmic reticulum), and the reactions and metabolites identifiers are listed in the table. MEMOTE scores before and after manual curation are given in the last column. Dark red highlights our reconstruction for the strain ATCC 17978. After manual curation, our model developed following our workflow in Fig 1 has the highest quality score and comes along with a minimal medium defined.

| | Availability | Used Identifiers | Growth by default mmol/($g_{DW}$ · h) | Compartments | MEMOTE | BioModels ID |
|---|---|---|---|---|---|---|
| **AbyMBEL891** [30] | BioModels | Customized | 119.0 | Cell | 20% + 17% | MODEL2406250010 |
| **AGORA** [32] | VMH | VMH | 134.0 | C, E | 42% + 37% | MODEL2406250011 |
| ***i*LP844** [31] | Suppl. Mat | ModelSeed | 15.88 | C, E, P | 37% + 21% | MODEL2406250005 |
| ***i*CN718** [33] | BiGG | BiGG | 1.31 | C, E, P, ER | 70% + 3% | MODEL2406250007 |
| ***i*ATCC19606** [34] | Suppl. Mat | KEGG | 46.34 | C, E | 14% + 44% | MODEL2406250008 |
| ***i*JS784** [36] | GitHub | ModelSeed | 0.0 | C, E, P | 41% + 18% | MODEL2406250006 |
| ***i*AB5075** [35] | Suppl. Mat | BiGG | 1. 729 | C, E, P | 17% + 50% | MODEL2406250009 |
| ***i*ACB23LX** | BioModels | BiGG | 0.5503 | C, E, P | 89% | MODEL2309120001 |

https://doi.org/10.1371/journal.ppat.1012528.t003

syntactically invalid or of older formats. Here, we systematically analyzed the quality of all seven currently existing GEMs, reporting their strengths and weaknesses and debugging them to finally build a curated, standardized, and updated collection. To do so, we developed a workflow with curation steps applicable to all models aiming at the standardization and usability of published GEMs by the community (Fig 6a). This closely follows the community-driven workflow published by Carey *et al.* for the reconstruction of reusable and translatable models [37]. The curation procedure includes a series of stages aiming at modifying data format, data amount, and information quality. It is important to note that no contextual modifications were conducted that could affect the model's prediction capabilities (see Materials and methods).

Five *A. baumannii* strains have been reconstructed throughout the years, with AYE and ATCC 19606 having two reconstructions each. All models are publicly stored and can be downloaded either from a database/repository [BioModels, Virtual Metabolic Human (VMH) [69], BiGG [70], and GitHub] or directly from the publication's additional material. The use of

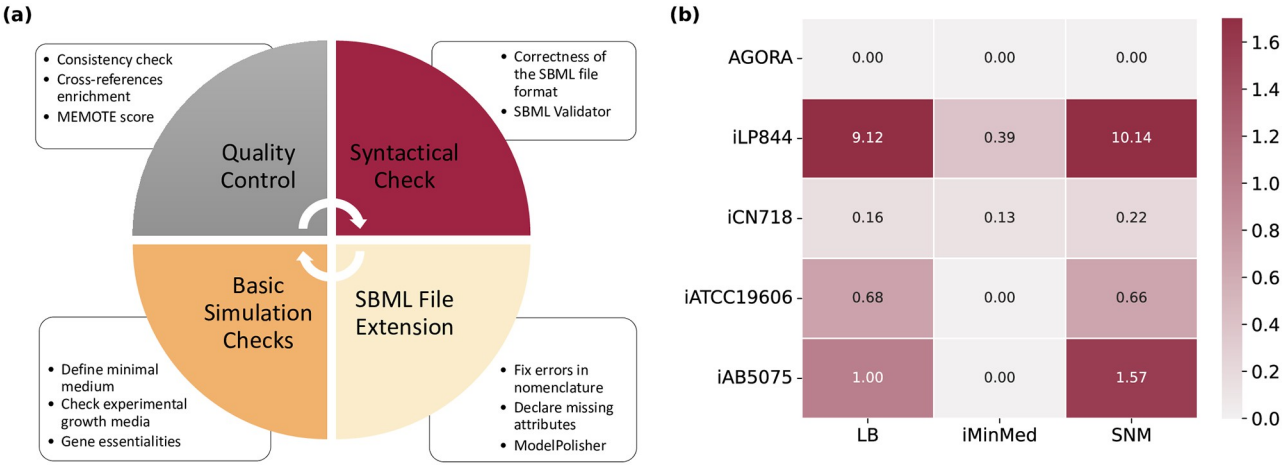


**Fig 6. Collection of strain-specific *A. baumannii* metabolic models. (a)** Debugging workflow to curate and evaluate already published models. Following the community standards, the existing *A. baumannii* models were curated and transformed into re-usable, simulatable, and translatable models. Quality controls and metabolic standardized tests were conducted using `MEMOTE`, while the validity of the file format and syntax were examined with the SBML Validator [46]. ModelPolisher enhanced the models with missing metadata. **(b)** *In silico*-derived growth rates in various media. The empirical and predicted growth rates of *i*ACB23LX are listed in Table 2.

https://doi.org/10.1371/journal.ppat.1012528.g006

distinct identifiers prevents the metabolic networks from being compared to each other. More specifically, *i*LP844 and *i*JS784 carry ModelSEED [71] identifiers for reactions and metabolites, while *i*CN718 and *i*AB5075 BiGG [70] identifiers. AbyMBEL891 uses distinct identifiers not supported by any database, and *i*ATCC19606 includes identifiers derived from KEGG [38]. Most of the models resulted in an unrealistic and inflated growth rate (reference: doubling time of the fastest growing organism *V. natriegens*) in their defined medium, while *i*JS784 showed a zero growth even when all imports were enabled (Table 3). Hence, this model was excluded from further analysis. For each of the remaining GEM, we defined the minimum growth requirements that result in a non-zero and realistic objective value. For instance, the AGORA model required at least 21 compounds (mostly metal ions), while oxygen was sufficient for AbyMBEL891 to simulate a non-zero growth (S5 Table).

Since these models should successfully reflect the bacterium's metabolic and growth capabilities (S2 Fig), we examined the flux through their biomass reaction in various growth media known to induce *A. baumannii* growth (Fig 6b). The majority resulted in a biomass flux of 0.0 mmol/($g_{DW}$ · h) in the *i*MinMed, while the AGORA model could not simulate growth in LB and SNM as well. Thus, we investigated and identified minimal medium supplementations needed to enable cellular biomass production. As already mentioned, *i*JS784 was excluded from further examination (Table 3), together with AbyMBEL891 that debilitated the analysis due to its non-standardized identifiers and its missing genes and GPRs. When the *i*MinMed for *i*ATCC19606 and *i*AB5075 was supplemented with D-alanine and D-glucose 6-phospahte as well as guanosine 5'-phosphate (GMP), respectively, their biomass reactions carried a positive flux rate of 0.5279 mmol/($g_{DW}$ · h) and 0.6477 mmol/($g_{DW}$ · h). Supplementation of meso-2,6-diaminoheptanedioate, menaquinone-8, niacinamide, heme, siroheme, and spermidine into the medium of the AGORA model resulted in a positive growth rate of 1.9430 mmol/($g_{DW}$ · h). Similarly, when supplementing the SNM with glycyl-L-asparagine, the derived growth rate was 1.5020 mmol/($g_{DW}$ · h), while the *i*MinMed needed to be extended with 12 additional components (resulted growth rate: 1.2789 mmol/($g_{DW}$ · h)). Lastly, like with *i*ACB23LX, the LB medium, together with FBA and MOMA, were applied to detect lethal genes in all models (S6 and S7 Tables). Despite remarkable efforts, we could not derive a mapping scheme between the strain-specific gene identifiers of *i*LP844 and *i*ATCC19606 to resolve PROKKA or HMPREF identifiers. Similar issues arose with *i*AB5075. Thus, a strain-wise comparison of essential genes would be feasible only for the strain ATCC 17978. Subsequently, we examined which genes were necessary for growth among the remaining models across three different strains: AYE (*i*CN718), ATCC 17978 (*i*ACB23LX), and AB0057 (AGORA). Totally, 392 genes were identified as essential, while 34 occurred in all three strains. For instance, when the genes encoding for dephospho-CoA kinase, phosphopantetheinyl transferase, shikimate kinase, or chorismate synthase were deleted from the three strains, no growth could be simulated in the LB medium. As already mentioned, the gene encoding the chorismate synthase has no human-like counterpart. This, together with the fact that it was detected to be vital for growth across three distinct strains, increases its potential to be a drug candidate for future therapies. Generally, most essential genes are members of the purine metabolism and encode various transferases. Besides this, the pantothenate and CoA biosynthesis and the amino acid metabolism were found to be a prominent target pathways for further drug development.

## Discussion

The historical timeline of past pandemics shows the imposed threat of bacteria in causing repetitive outbreaks with the highest death tolls [72], such as cholera and plague. By 2050, antimicrobial-resistant pathogens are expected to kill 10 million people annually [73], while the

antibiotics misuse accompanied by the ongoing Coronavirus Disease 2019 (COVID-19) crisis exacerbated this global threat. It is noteworthy that elevated morbidity rates were ascribed to bacterial co/secondary infections during previous viral disease outbreaks [74–76]. Hence, developing effective antibiotic regimens is of urgent importance. Here, we present the most recent and comprehensive ready-to-use blueprint GEM for the Gram-negative pathogen *A. baumannii*. For this, we created a workflow that applies to any living organism and ensures the reconstruction of high-quality models following the community standards. Our model, *i*ACB23LX, was able to simulate growth in SNM that mimics the human nasal niche, the experimentally defined medium LB, and the model-derived *i*MinMed. With *i*MinMed we denoted the minimal number of compounds needed to achieve non-zero growth. This medium contains totally 14 compounds, including transition metals and energy sources. Transition metals have been shown to participate in important biological processes and are vital for the survival of living organisms [50]. We confirmed the computationally predicted growth rates by comparing them to our empirically determined growth kinetics data. With this, we ensured that our model recapitulates growth phenotypes in media that reflect *Acinetobacter*-associated environments.

Furthermore, we validated *i*ACB23LX quantitatively and qualitatively using existing experimental data and observed remarkable improvements compared to precursory models. More specifically, our model predicted experimental Biolog growth phenotypes on various carbon sources with an overall agreement of 86.3%. This agreement is higher than the prediction capability of *i*ATCC19606 (84.3%) and *i*LP844 (84%), and comparable to that of *i*AB5075 (86.3%). Similarly, *i*ACB23LX exhibited 79.2% predictive accuracy on nitrogen sources tests, while this increases to 87.5% after further refinement. Improving and re-defining the biomass objective function (BOF) based on accurate strain-specific experimental data would be the next step to diminish the number of inconsistent predictions and to further improve the network and its predictive potential. During gene lethality analysis in LB medium, our model predicted 110 genes with MOMA to be essential, while 97 of them were also reported by FBA to impair the growth. Generally, after enriching the nutritional input with all available compounds (rich medium), less lethal genes resulted, meaning that *A. baumannii* undergoes metabolic alterations when nutrients are lacking. Our *in silico* results, when compared to five different strain-specific gene essentiality data [57, 68, 77–79], achieved accuracies between 88.60% and 88.92%. The predictive accuracies are remarkably higher than all GEMs built for *A. baumannii* (e.g., 80.22% for *i*CN718 and 72% for *i*LP844), except *i*AB5075 which performed comparably. This comprehensive analysis ensures that our model is well-validated and highly reliable, making it a valuable tool for predicting gene essentiality in various biological and experimental settings.

Subsequently, we examined more carefully our false negative predictions and searched for putative drug targets that could be employed for future therapeutics. More specifically, we focused on genes found to be essential for growth and encode proteins with no human counterparts (S4 Table). Our study highlighted EPSP and chorismate synthases from the shikimate pathway as prominent target candidates with no correlation to the human proteome. Several knockout studies have highlighted the importance of enzymes from the shikimate metabolism as potential targets against infections caused by threatening microorganisms, e.g., *Mycobacterium tuberculosis* [80], *Plasmodium falciparum* [81], and *Yersinia enterocolitica* [82]. Umland *et al*. identified these two gene products as essential in an *in vivo* study using a clinical isolate of *A. baumannii* (AB307-0294) and a rat abscess infection model [83]. This increases the confidence of our results and indicates that genes found to be essential *in silico* should be considered as potential antimicrobial targets. Moreover, our predicted target DHFR has been

extensively studied as a primary target for antibacterial and anticancer drug development, given its pivotal role in nucleotide biosynthesis [84–88].

Trimethoprim (TMP), an antifolate antibacterial agent, selectively inhibits the bacterial DHFR, a crucial enzyme catalyzing the tetrahydrofolic acid (THF) formation. Sulfamethoxazole (SMX), a bacteriostatic sulfonamide antibiotic, competitively inhibits dihydropteroate synthase, responsible for the formation of dihydrofolate (DHF). Together as cotrimoxazole or TMP-SMX, both compounds effectively treat bacterial infections by collectively inhibiting folic acid synthesis, essential for bacterial growth and replication [89, 90]. Further studies have shown that antifolates effectively inhibit *A. baumannii* DHFR, demonstrating potent antibacterial activity against multidrug-resistant strains and highlighting their potential for further antibiotic development [91, 92]. Finally, targeting folate biosynthesis is a well-established strategy against infectious diseases due to its absence in higher eukaryotic organisms. Altogether, selectively targeting bacterial proteins vital for key cellular functions, such as cell wall biosynthesis, translation, and deoxyribonucleic acid (DNA) replication, is a well-established strategy in antibiotic development. Similarly, numerous studies have suggested one of our further candidates, riboflavin, as a potential antimicrobial agent for further investigation [63]. Additionally, the Entner–Doudoroff pathway, in which our candidate targets phosphogluconate dehydratase and KDPG aldolase act to produce pyruvate, is similar to glycolysis but involves different enzymes. This pathway has been firstly discovered in *P. saccharophila* [65] and later in *E. coli* [93]. Meanwhile, it is vital for the survival of further pathogenic microorganisms, like *Neisseria gonorrhoeae*, *K. pneumoniae*, and *P. aeruginosa* [94–96]. However, these targets have not yet been examined in *Acinetobacter* species and could be a source of antimicrobial therapeutic strategies. Hence, these biosynthetic routes could be a valuable resource for targets to fight bacterial infectious diseases. Finally, we investigated the druggability of our essential non-homologous genes. We searched the DrugBank database to find compounds known to inhibit these genes and that are already approved by the Food and Drug Administration (FDA). Our analysis resulted in drugs that have been found to interact with the gene product of interest; however their pharmacological action is yet unknown. We further probed the hypothetical and putative non-homologous genes against the DrugBank's sequence database to find homologous proteins and determine their activity. Also in this case, the resulted drugs were listed with still undetermined pharmacological action. These putative and yet unexplored targets with inhibitory potential are of great interest in the context of developing new classes of antibiotics. Overall, our model reached a `MEMOTE` score of 89%, which is the highest score reported for this organism.

Moreover, we improved and assessed all previously published models and created the first curated strain-specific collection of metabolic networks for *A. baumannii*. We created a debugging workflow consisting of four major steps to systematically analyze and curate constraint-based models focusing on their standardization and the FAIR data principles. We applied this workflow and curated a total of seven metabolic models for *A. baumannii*. In addition, most of the models simulated growth rates by default that were unrealistic when compared to the fastest growing organism [45]. Therefore, we determined the minimal number of components needed for these models to result in non-inflated biomass production rates. The defined minimal media were mostly composed of metal ions (e.g., cobalt, iron, magnesium) that are essential for bacterial growth. For the model *i*JS784, the minimization process was infeasible; thus, the model was not considered for further analysis. We also examined the growth ability of these models in three media (SNM, LB, and *i*MinMed) and compared them to our model, *i*ACB23LX. When the models simulated a zero flux through the biomass reaction, we continued by detecting the minimal amount of metabolites supplemented in the medium that resulted in a non-zero growth rate. These would enable the detection of gaps and assist in future improvement of the models. It is important to note here that with this curation, we

opted for a systematical assessment of the previously reconstructed models and the detection of their assets and liabilities. Consequently, we did not undertake any contextual modification that could alter the models' predictive capabilities. Finally, we predicted lethal genes among comparable and simulatable models of *A. baumannii*. Our analysis incorporated three strains (AYE, AB0057, and ATCC 17978), and we examined the effect of genetic variation across strains in the gene essentiality. We highlighted once again the shikimate pathway, as well as the purine metabolism, the pantothenate, and CoA biosynthesis, and the amino acid metabolism as candidate routes to consider for future new classes of antibacterial drugs with potential effect across multiple *A. baumannii* strains. The curated models, together with our model, would benefit the future prediction of candidate lethal genes by reducing the considerable resources needed for classical whole-genome essentiality screenings. All in all, this collection of simulation-ready models will forward the selection of a suitable metabolic network based on individual research questions and help define the entire species and new hypothesis.

Our new metabolic reconstruction and the curated collection of further strain-specific models will guide the formulation of ground-breaking and reliable model-driven hypotheses about this pathogen and help examine the diversity in the metabolic behavior of different *A. baumannii* species in response to genetic and environmental alterations. Additionally, they can be utilized as knowledge bases to detect critical pathways related to responses against multiple antibiotic treatments. This will ultimately strengthen the development of advanced precision antimicrobial control strategies against multidrug-resistant (MDR) *A. baumannii* strains.

Taken together, our workflows and models can be employed to expand this collection further with additional standardized strain-specific metabolic reconstructions to finally define the core and pan metabolic capabilities of *A. baumannii*.

## Supporting information

**S1 Fig. Oxygen-producing and -consuming reactions found in *i*ACB23LX together with their anaerobic fluxes.** All flux rates are written in orange and are given in mmol/($g_{DW}$ · h). The reaction abbreviations are as follows: `O2tpp`, $O_2$ transport via diffusion between periplasm and cytosol; `CATpp`, periplasmatic catalase; `H2O2tex`, hydrogen peroxide transport via diffusion; `CAT`, catalase; `O2tex`, $O_2$ transport via diffusion between periplasm and extracellular space; `EX_h2o2_e`, hydrogen peroxide exchange and `EX_o2_e`, $O_2$ exchange. Figure generated with Escher [109].
(TIF)

**S2 Fig. Experimentally-derived growth curves of *A. baumannii*.** The growth curves for *A. baumannii* strains AB5075, ATCC 73217978, ATCC 19606, and AYE were measured in LB and SNM. Additionally, the *in silico*-defined minimal medium (*i*MinMed) was tested for all strains.
(TIF)

**S3 Fig. Comparative analysis of essential genes predicted by *i*ACB23LX versus those identified in Tn-seq libraries [57, 68, 77–79]. (a)** Metabolic subsystems distribution of all essential genes reported in various Tn-seq studies and predicted using *i*ACB23LX (true negatives). **(b)** Venn diagrams of essential genes from five examined Tn-seq datasets compared to essential genes predicted by the model developed in this study.
(TIF)

**S1 Table. *In silico* formulations of examined media compositions.** Metabolites are described by BiGG [70] identifiers.
(XLSX)

**S2 Table. *In silico* gene knockout results using FBA.** The ratio column describes the growth rate change before and after the respective knockout.
(XLSX)

**S3 Table. *In silico* gene knockout results using MOMA.** The ratio column describes the growth rate change before and after the respective knockout.
(XLSX)

**S4 Table. Metabolic genes found to be essential for growth in *i*ACB23LX and encode proteins with no human counterparts.**
(XLSX)

**S5 Table. Computationally-defined minimal growth media for previously published models.** Due to inflated growth rates in most published *A. baumannii* GEMs, we established minimal media supporting non-zero biomass flux.
(XLSX)

**S6 Table. Gene lethality predictions using previously published *A. baumannii* models and FBA.**
(CSV)

**S7 Table. Gene lethality predictions using previously published *A. baumannii* models and MOMA.** This offers a complementary perspective on the essential genes in the organism's metabolism.
(CSV)

**S8 Table. Summary of essential genes predicted by *i*ACB23LX and confirmed in Tn-seq libraries [57, 68, 77–79].** Five independent Tn-seq datasets were utilized for the comparison. Both FBA and MOMA were used with the LB medium defined to predict essential genes. The table also includes the intersection of essential genes identified by both methods, along with their associated orthologs in the case of different studied genomes. The computed accuracies verified the high predictive performance of our model.
(XLSX)

## Acknowledgments

The authors also thank Dr. Bernhard Krismer for providing the synthetic nasal medium.

## Author Contributions

**Conceptualization:** Nantia Leonidou, Andreas Dräger.

**Data curation:** Nantia Leonidou.

**Formal analysis:** Nantia Leonidou, Lea Friedrich.

**Funding acquisition:** Monika S. Schütz, Andreas Dräger.

**Investigation:** Nantia Leonidou, Lea Friedrich.

**Methodology:** Nantia Leonidou, Yufan Xia.

**Project administration:** Monika S. Schütz, Andreas Dräger.

**Resources:** Monika S. Schütz, Andreas Dräger.

**Software:** Nantia Leonidou, Yufan Xia.

**Supervision:** Monika S. Schütz, Andreas Dräger.

**Validation:** Nantia Leonidou.

**Visualization:** Nantia Leonidou.

**Writing – original draft:** Nantia Leonidou.

**Writing – review & editing:** Nantia Leonidou, Monika S. Schütz, Andreas Dräger.

## References

1. Magiorakos AP, Srinivasan A, Carey RB, Carmeli Y, Falagas M, Giske C, et al. Multidrug-resistant, extensively drug-resistant and pandrug-resistant bacteria: an international expert proposal for interim standard definitions for acquired resistance. Clinical microbiology and infection. 2012; 18(3):268–281. https://doi.org/10.1111/j.1469-0691.2011.03570.x PMID: 21793988
2. Murray CJ, Ikuta KS, Sharara F, Swetschinski L, Aguilar GR, Gray A, et al. Global burden of bacterial antimicrobial resistance in 2019: a systematic analysis. The Lancet. 2022; 399(10325):629–655. https://doi.org/10.1016/S0140-6736(21)02724-0 PMID: 35065702
3. Fournier PE, Richet H. The epidemiology and control of *Acinetobacter baumannii* in health care facilities. Clinical Infectious Diseases. 2006; 42:692–699. https://doi.org/10.1086/500202 PMID: 16447117
4. Dijkshoorn L, Nemec A, Seifert H. An increasing threat in hospitals: multidrug-resistant *Acinetobacter baumannii*. Nature Reviews Microbiology 2007 5:12. 2007; 5:939–951. https://doi.org/10.1038/nrmicro1789 PMID: 18007677
5. Peleg AY, Seifert H, Paterson DL. *Acinetobacter baumannii*: Emergence of a Successful Pathogen. Clinical Microbiology Reviews. 2008; 21:538. https://doi.org/10.1128/CMR.00058-07 PMID: 18625687
6. Ibrahim S, Al-Saryi N, Al-Kadmy IMS, Aziz SN. Multidrug-resistant *Acinetobacter baumannii* as an emerging concern in hospitals. Molecular Biology Reports. 2021; 48:6987. https://doi.org/10.1007/S11033-021-06690-6 PMID: 34460060
7. Bogaerts P, Naas T, Wybo I, Bauraing C, Soetens O, Piérard D, et al. Outbreak of infection by carbapenem-resistant *Acinetobacter baumannii* producing the carbapenemase OXA-58 in Belgium. Journal of clinical microbiology. 2006; 44(11):4189–4192. https://doi.org/10.1128/JCM.00796-06 PMID: 16957031
8. Cai B, Echols R, Magee G, Arjona Ferreira JC, Morgan G, Ariyasu M, et al. Prevalence of carbapenem-resistant Gram-negative infections in the United States predominated by *Acinetobacter baumannii* and *Pseudomonas aeruginosa*. In: Open forum infectious diseases. vol. 4. Oxford University Press; 2017.
9. Iovleva A, Mustapha MM, Griffith MP, Komarow L, Luterbach C, Evans DR, et al. Carbapenem-Resistant *Acinetobacter baumannii* in US hospitals: diversification of circulating lineages and antimicrobial resistance. Mbio. 2022; 13(2):e02759–21. https://doi.org/10.1128/mbio.02759-21 PMID: 35311529
10. Damaceno Q, Nicoli JR, Oliveira A. Variability of cutaneous and nasal population levels between patients colonized and infected by multidrug-resistant bacteria in two Brazilian intensive care units. SAGE Open Medicine. 2015; 3:2050312114566668. https://doi.org/10.1177/2050312114566668 PMID: 26770762
11. Liou ML, Chen KH, Yeh HL, Lai CY, Chen CH. Persistent nasal carriers of *Acinetobacter baumannii* in long-term-care facilities. American journal of infection control. 2017; 45(7):723–727. https://doi.org/10.1016/j.ajic.2017.02.005 PMID: 28284750
12. Chen CH, Liou ML, Lee CY, Chang MC, Kuo HY, Chang TH. Diversity of nasal microbiota and its interaction with surface microbiota among residents in healthcare institutes. Scientific reports. 2019; 9(1):1–10. https://doi.org/10.1038/s41598-019-42548-5 PMID: 30992494
13. Rangel K, Chagas TPG, De-Simone SG. *Acinetobacter baumannii* infections in times of COVID-19 pandemic. Pathogens. 2021; 10(8):1006. https://doi.org/10.3390/pathogens10081006 PMID: 34451470
14. Contou D, Claudinon A, Pajot O, Micaëlo M, Longuet Flandre P, Dubert M, et al. Bacterial and viral co-infections in patients with severe SARS-CoV-2 pneumonia admitted to a French ICU. Annals of intensive care. 2020; 10(1):1–9. https://doi.org/10.1186/s13613-020-00736-x PMID: 32894364
15. Lima WG, Brito JCM, da Cruz Nizer WS. Ventilator-associated pneumonia (VAP) caused by carbapenem-resistant *Acinetobacter baumannii* in patients with COVID-19: Two problems, one solution? Medical hypotheses. 2020; 144:110139. https://doi.org/10.1016/j.mehy.2020.110139 PMID: 32758905

16. Russo A, Gavaruzzi F, Ceccarelli G, Borrazzo C, Oliva A, Alessandri F, et al. Multidrug-resistant *Acinetobacter baumannii* infections in COVID-19 patients hospitalized in intensive care unit. Infection. 2022; 50(1):83–92. https://doi.org/10.1007/s15010-021-01643-4 PMID: 34176088

17. Seifert H, Dijkshoorn L, Gerner-Smidt P, Pelzer N, Tjernberg I, Vaneechoutte M. Distribution of *Acinetobacter* species on human skin: comparison of phenotypic and genotypic identification methods. Journal of clinical microbiology. 1997; 35(11):2819–2825.

18. Dijkshoorn L, Van Aken E, Shunburne L, Van Der Reijden T, Bernards A, Nemec A, et al. Prevalence of *Acinetobacter baumannii* and other *Acinetobacter* spp. in faecal samples from non-hospitalised individuals. Clinical microbiology and infection. 2005; 11(4):329–332. https://doi.org/10.1111/j.1469-0691.2005.01093.x PMID: 15760432

19. Howard A, O'Donoghue M, Feeney A, Sleator RD. *Acinetobacter baumannii*: an emerging opportunistic pathogen. Virulence. 2012; 3(3):243–250. https://doi.org/10.4161/viru.19700 PMID: 22546906

20. Smith MG, Gianoulis TA, Pukatzki S, Mekalanos JJ, Ornston LN, Gerstein M, et al. New insights into *Acinetobacter baumannii* pathogenesis revealed by high-density pyrosequencing and transposon mutagenesis. Genes & development. 2007; 21(5):601–614. https://doi.org/10.1101/gad.1510307 PMID: 17344419

21. Weber BS, Miyata ST, Iwashkiw JA, Mortensen BL, Skaar EP, Pukatzki S, et al. Genomic and functional analysis of the type VI secretion system in *Acinetobacter*. PloS one. 2013; 8(1):e55142. https://doi.org/10.1371/journal.pone.0055142 PMID: 23365692

22. Bisaro F, Shuman HA, Feldman MF, Gebhardt MJ, Pukatzki S. *Acinetobacter baumannii* ATCC 17978 encodes a microcin system with antimicrobial properties for contact-independent competition. Microbiology. 2023; 169(6):001346. https://doi.org/10.1099/mic.0.001346 PMID: 37289493

23. Adams MD, Goglin K, Molyneaux N, Hujer KM, Lavender H, Jamison JJ, et al. Comparative genome sequence analysis of multidrug-resistant *Acinetobacter baumannii*. Journal of bacteriology. 2008; 190 (24):8053–8064. https://doi.org/10.1128/JB.00834-08 PMID: 18931120

24. Valentine SC, Contreras D, Tan S, Real LJ, Chu S, Xu HH. Phenotypic and molecular characterization of *Acinetobacter baumannii* clinical isolates from nosocomial outbreaks in Los Angeles County, California. Journal of clinical microbiology. 2008; 46(8):2499–2507. https://doi.org/10.1128/JCM.00367-08 PMID: 18524965

25. Antunes LC, Imperi F, Carattoli A, Visca P. Deciphering the multifactorial nature of *Acinetobacter baumannii* pathogenicity. PloS one. 2011; 6(8):e22674. https://doi.org/10.1371/journal.pone.0022674 PMID: 21829642

26. Farrugia DN, Elbourne LD, Hassan KA, Eijkelkamp BA, Tetu SG, Brown MH, et al. The complete genome and phenome of a community-acquired *Acinetobacter baumannii*. PloS one. 2013; 8(3): e58628. https://doi.org/10.1371/journal.pone.0058628 PMID: 23527001

27. Jacobs AC, Thompson MG, Black CC, Kessler JL, Clark LP, McQueary CN, et al. AB5075, a highly virulent isolate of *Acinetobacter baumannii*, as a model strain for the evaluation of pathogenesis and antimicrobial treatments. MBio. 2014; 5(3):10–1128. https://doi.org/10.1128/mBio.01076-14 PMID: 24865555

28. Thiele I, Palsson BØ. A protocol for generating a high-quality genome-scale metabolic reconstruction. Nature protocols. 2010; 5(1):93–121. https://doi.org/10.1038/nprot.2009.203 PMID: 20057383

29. Oberhardt MA, Palsson BØ, Papin JA. Applications of genome-scale metabolic reconstructions. Molecular systems biology. 2009; 5(1):320. https://doi.org/10.1038/msb.2009.77 PMID: 19888215

30. Kim HU, Kim TY, Lee SY. Genome-scale metabolic network analysis and drug targeting of multi-drug resistant pathogen *Acinetobacter baumannii* AYE. Molecular BioSystems. 2010; 6(2):339–348. https://doi.org/10.1039/b916446d PMID: 20094653

31. Presta L, Bosi E, Mansouri L, Dijkshoorn L, Fani R, Fondi M. Constraint-based modeling identifies new putative targets to fight colistin-resistant *A. baumannii* infections. Scientific reports. 2017; 7(1):1–12. https://doi.org/10.1038/s41598-017-03416-2 PMID: 28623298

32. Magnúsdóttir S, Heinken A, Kutt L, Ravcheev DA, Bauer E, Noronha A, et al. Generation of genome-scale metabolic reconstructions for 773 members of the human gut microbiota. Nature biotechnology. 2017; 35(1):81–89. https://doi.org/10.1038/nbt.3703 PMID: 27893703

33. Norsigian CJ, Kavvas E, Seif Y, Palsson BO, Monk JM. iCN718, an updated and improved genome-scale metabolic network reconstruction of *Acinetobacter baumannii* AYE. Frontiers in genetics. 2018; 9:121. https://doi.org/10.3389/fgene.2018.00121 PMID: 29692801

34. Zhu Y, Zhao J, Maifiah MHM, Velkov T, Schreiber F, Li J. Metabolic responses to polymyxin treatment in *Acinetobacter baumannii* ATCC 19606: integrating transcriptomics and metabolomics with genome-scale metabolic modeling. Msystems. 2019; 4(1):e00157–18. https://doi.org/10.1128/mSystems.00157-18 PMID: 30746493

35. Zhao J, Zhu Y, Han J, Lin YW, Aichem M, Wang J, et al. Genome-scale metabolic modeling reveals metabolic alterations of multidrug-resistant *Acinetobacter Baumannii* in a murine bloodstream infection model. Microorganisms. 2020; 8(11):1793. https://doi.org/10.3390/microorganisms8111793 PMID: 33207684

36. Barbosa JSC. Genome-scale reconstruction of the metabolic network iJS784 for *Acinetobacter baumannii* strain ATCC 17978 to address drug target prioritization [dissertation]. National Laboratory for Scientific Computing, Brazil; 2020. Available from: http://bdtd.ibict.br/vufind/Record/LNCC_66db4adf05fede6c0e4bf5b7e6cd9069.

37. Carey MA, Dräger A, Beber ME, Papin JA, Yurkovich JT. Community standards to facilitate development and address challenges in metabolic modeling. Molecular Systems Biology. 2020; 16(8):e9235. https://doi.org/10.15252/msb.20199235 PMID: 32845080

38. Kanehisa M, Furumichi M, Sato Y, Ishiguro-Watanabe M, Tanabe M. KEGG: integrating viruses and cellular organisms. Nucleic acids research. 2020; https://doi.org/10.1093/nar/gkaa970 PMID: 33125081

39. Machado D, Andrejev S, Tramontano M, Patil KR. Fast automated reconstruction of genome-scale metabolic models for microbial species and communities. Nucleic acids research. 2018; 46(15):7542–7553. https://doi.org/10.1093/nar/gky537 PMID: 30192979

40. Keating SM, Waltemath D, König M, Zhang F, Dräger A, Chaouiya C, et al. SBML Level 3: an extensible format for the exchange and reuse of biological models. Molecular Systems Biology. 2020; 16(8): e9110. https://doi.org/10.15252/msb.20199110 PMID: 32845085

41. Fritzemeier CJ, Hartleb D, Szappanos B, Papp B, Lercher MJ. Erroneous energy-generating cycles in published genome scale metabolic networks: Identification and removal. PLoS computational biology. 2017; 13(4):e1005494. https://doi.org/10.1371/journal.pcbi.1005494 PMID: 28419089

42. Jupp S, Burdett T, Leroy C, Parkinson HE. A new Ontology Lookup Service at EMBL-EBI. SWAT4LS. 2015; 2:118–119.

43. Leonidou N, Fritze E, Renz A, Dräger A. SBOannotator: a Python Tool for the Automated Assignment of Systems Biology Ontology Terms. Bioinformatics. 2023; p. btad437. https://doi.org/10.1093/bioinformatics/btad437 PMID: 37449910

44. yWorks GmbH. yEd. 2019;.

45. Lieven C, Beber ME, Olivier BG, Bergmann FT, Ataman M, Babaei P, et al. MEMOTE for standardized genome-scale metabolic model testing. Nature biotechnology. 2020; 38(3):272–276. https://doi.org/10.1038/s41587-020-0446-y PMID: 32123384

46. Bornstein BJ, Keating SM, Jouraku A, Hucka M. LibSBML: an API library for SBML. Bioinformatics. 2008; 24(6):880–881. https://doi.org/10.1093/bioinformatics/btn051 PMID: 18252737

47. König M. matthiaskoenig/fbc curation: fbc curation-v0.0.6; 2020. Available from: https://doi.org/10.5281/zenodo.3711541.

48. Hucka M, Bergmann FT, Chaouiya C, Dräger A, Hoops S, Keating SM, et al. Systems Biology Markup Language (SBML): Language Specification for Level 3 Version 2 Core Release 2. Journal of Integrative Bioinformatics. 2019; 16(2):1. https://doi.org/10.1515/jib-2019-0021 PMID: 31219795

49. Mishra S, Imlay J. Why do bacteria use so many enzymes to scavenge hydrogen peroxide? Archives of biochemistry and biophysics. 2012; 525(2):145–160. https://doi.org/10.1016/j.abb.2012.04.014 PMID: 22609271

50. Hood MI, Skaar EP. Nutritional immunity: transition metals at the pathogen–host interface. Nature Reviews Microbiology. 2012; 10(8):525–537. https://doi.org/10.1038/nrmicro2836 PMID: 22796883

51. Mortensen BL, Skaar EP. The contribution of nutrient metal acquisition and metabolism to *Acinetobacter baumannii* survival within the host. Frontiers in cellular and infection microbiology. 2013; 3:95. https://doi.org/10.3389/fcimb.2013.00095 PMID: 24377089

52. Hood MI, Mortensen BL, Moore JL, Zhang Y, Kehl-Fie TE, Sugitani N, et al. Identification of an *Acinetobacter baumannii* zinc acquisition system that facilitates resistance to calprotectin-mediated zinc sequestration. PLoS pathogens. 2012; 8(12):e1003068. https://doi.org/10.1371/journal.ppat.1003068 PMID: 23236280

53. Raman K, Rajagopalan P, Chandra N. Flux balance analysis of mycolic acid pathway: targets for antitubercular drugs. PLoS computational biology. 2005; 1(5):e46. https://doi.org/10.1371/journal.pcbi.0010046 PMID: 16261191

54. Ma S, Minch KJ, Rustad TR, Hobbs S, Zhou SL, Sherman DR, et al. Integrated modeling of gene regulatory and metabolic networks in *Mycobacterium tuberculosis*. PLoS computational biology. 2015; 11 (11):e1004543. https://doi.org/10.1371/journal.pcbi.1004543 PMID: 26618656

55. Lee DS, Burd H, Liu J, Almaas E, Wiest O, Barabási AL, et al. Comparative genome-scale metabolic reconstruction and flux balance analysis of multiple *Staphylococcus aureus* genomes identify novel

antimicrobial drug targets. Journal of bacteriology. 2009; 191(12):4015–4024. https://doi.org/10.1128/JB.01743-08 PMID: 19376871

56. Seif Y, Monk JM, Mih N, Tsunemoto H, Poudel S, Zuniga C, et al. A computational knowledge-base elucidates the response of *Staphylococcus aureus* to different media types. PLoS computational biology. 2019; 15(1):e1006644. https://doi.org/10.1371/journal.pcbi.1006644 PMID: 30625152

57. Wang N, Ozer EA, Mandel MJ, Hauser AR. Genome-wide identification of *Acinetobacter baumannii* genes necessary for persistence in the lung. MBio. 2014; 5(3):e01163–14. https://doi.org/10.1128/mBio.01163-14 PMID: 24895306

58. Ebrahim A, Lerman JA, Palsson BO, Hyduke DR. COBRApy: constraints-based reconstruction and analysis for python. BMC systems biology. 2013; 7(1):1–6. https://doi.org/10.1186/1752-0509-7-74 PMID: 23927696

59. Orth JD, Thiele I, Palsson BØ. What is flux balance analysis? Nature biotechnology. 2010; 28(3):245–248. https://doi.org/10.1038/nbt.1614 PMID: 20212490

60. Segre D, Vitkup D, Church GM. Analysis of optimality in natural and perturbed metabolic networks. Proceedings of the National Academy of Sciences. 2002; 99(23):15112–15117. https://doi.org/10.1073/pnas.232349399 PMID: 12415116

61. Barh D, Tiwari S, Jain N, Ali A, Santos AR, Misra AN, et al. In silico subtractive genomics for target identification in human bacterial pathogens. Drug Development Research. 2011; 72(2):162–177. https://doi.org/10.1002/ddr.20413

62. Bentley R, Haslam E. The shikimate pathway—a metabolic tree with many branches. Critical reviews in biochemistry and molecular biology. 1990; 25(5):307–384. https://doi.org/10.3109/10409239009090615 PMID: 2279393

63. Farah N, Chin VK, Chong PP, Lim WF, Lim CW, Basir R, et al. Riboflavin as a promising antimicrobial agent? A multi-perspective review. Current Research in Microbial Sciences. 2022; p. 100111. https://doi.org/10.1016/j.crmicr.2022.100111 PMID: 35199072

64. Meloche H, Wood W. The mechanism of 6-phosphogluconic dehydrase. Journal of Biological Chemistry. 1964; 239(10):3505–3510. https://doi.org/10.1016/S0021-9258(18)97751-3 PMID: 14245409

65. Entner N, Doudoroff M. Glucose and gluconic acid oxidation of *Pseudomonas saccharophila*. J Biol Chem. 1952; 196(2):853–862. https://doi.org/10.1016/S0021-9258(19)52415-2

66. Wishart DS, Feunang YD, Guo AC, Lo EJ, Marcu A, Grant JR, et al. DrugBank 5.0: a major update to the DrugBank database for 2018. Nucleic acids research. 2018; 46(D1):D1074–D1082. https://doi.org/10.1093/nar/gkx1037 PMID: 29126136

67. Dorsey CW, Tomaras AP, Actis LA. Genetic and phenotypic analysis of *Acinetobacter baumannii* insertion derivatives generated with a transposome system. Applied and Environmental Microbiology. 2002; 68(12):6353–6360.

68. Gallagher LA, Ramage E, Weiss EJ, Radey M, Hayden HS, Held KG, et al. Resources for genetic and genomic analysis of emerging pathogen *Acinetobacter baumannii*. Journal of bacteriology. 2015; 197(12):2027–2035. https://doi.org/10.1128/JB.00131-15 PMID: 25845845

69. Noronha A, Modamio J, Jarosz Y, Guerard E, Sompairac N, Preciat G, et al. The Virtual Metabolic Human database: integrating human and gut microbiome metabolism with nutrition and disease. Nucleic acids research. 2019; 47(D1):D614–D624. https://doi.org/10.1093/nar/gky992 PMID: 30371894

70. Norsigian CJ, Pusarla N, McConn JL, Yurkovich JT, Dräger A, Palsson BO, et al. BiGG Models 2020: multi-strain genome-scale models and expansion across the phylogenetic tree. Nucleic Acids Research. 2019; 48(D1). https://doi.org/10.1093/nar/gkz1054 PMID: 31696234

71. Henry CS, DeJongh M, Best AA, Frybarger PM, Linsay B, Stevens RL. High-throughput generation, optimization and analysis of genome-scale metabolic models. Nature biotechnology. 2010; 28(9):977–982. https://doi.org/10.1038/nbt.1672 PMID: 20802497

72. Piret J, Boivin G. Pandemics throughout history. Frontiers in microbiology. 2021; 11:631736. https://doi.org/10.3389/fmicb.2020.631736 PMID: 33584597

73. O'Neill J, et al. Review on antimicrobial resistance. Antimicrobial resistance: tackling a crisis for the health and wealth of nations. 2014;(4).

74. Chien YW, Klugman KP, Morens DM. Bacterial pathogens and death during the 1918 influenza pandemic. New England Journal of Medicine. 2009; 361(26):2582–2583. https://doi.org/10.1056/NEJMc0908216 PMID: 20032332

75. Sheng ZM, Chertow DS, Ambroggio X, McCall S, Przygodzki RM, Cunningham RE, et al. Autopsy series of 68 cases dying before and during the 1918 influenza pandemic peak. Proceedings of the National Academy of Sciences. 2011; 108(39):16416–16421. https://doi.org/10.1073/pnas.1111179108 PMID: 21930918

**76.** Morris DE, Cleary DW, Clarke SC. Secondary bacterial infections associated with influenza pandemics. Frontiers in microbiology. 2017; 8:1041. https://doi.org/10.3389/fmicb.2017.01041 PMID: 28690590

**77.** Geisinger E, Mortman NJ, Dai Y, Cokol M, Syal S, Farinha A, et al. Antibiotic susceptibility signatures identify potential antimicrobial targets in the *Acinetobacter baumannii* cell envelope. Nature communications. 2020; 11(1):4522. https://doi.org/10.1038/s41467-020-18301-2 PMID: 32908144

**78.** Bai J, Dai Y, Farinha A, Tang AY, Syal S, Vargas-Cuebas G, et al. Essential gene analysis in *Acinetobacter baumannii* by high-density transposon mutagenesis and CRISPR interference. Journal of bacteriology. 2021; 203(12):10–1128. https://doi.org/10.1128/jb.00565-20 PMID: 33782056

**79.** Bai J, Raustad N, Denoncourt J, van Opijnen T, Geisinger E. Genome-wide phage susceptibility analysis in *Acinetobacter baumannii* reveals capsule modulation strategies that determine phage infectivity. PLoS Pathogens. 2023; 19(6):e1010928. https://doi.org/10.1371/journal.ppat.1010928 PMID: 37289824

**80.** Parish T, Stoker NG. The common aromatic amino acid biosynthesis pathway is essential in *Mycobacterium tuberculosis*. Microbiology. 2002; 148(10):3069–3077. https://doi.org/10.1099/00221287-148-10-3069 PMID: 12368440

**81.** Tapas S, Kumar A, Dhindwal S, Kumar P, et al. Structural analysis of chorismate synthase from *Plasmodium falciparum*: a novel target for antimalaria drug discovery. International journal of biological macromolecules. 2011; 49(4):767–777. https://doi.org/10.1016/j.ijbiomac.2011.07.011 PMID: 21801743

**82.** Bowe F, O'Gaora P, Maskell D, Cafferkey M, Dougan G. Virulence, persistence, and immunogenicity of *Yersinia enterocolitica* O:8 aroA mutants. Infection and immunity. 1989; 57(10):3234–3236.

**83.** Umland TC, Schultz LW, MacDonald U, Beanan JM, Olson R, Russo TA. In vivo-validated essential genes identified in *Acinetobacter baumannii* by using human ascites overlap poorly with essential genes detected on laboratory media. MBio. 2012; 3(4):e00113–12. https://doi.org/10.1128/mBio.00113-12 PMID: 22911967

**84.** Zhang Y, Chowdhury S, Rodrigues JV, Shakhnovich E. Development of antibacterial compounds that constrain evolutionary pathways to resistance. Elife. 2021; 10:e64518. https://doi.org/10.7554/eLife.64518 PMID: 34279221

**85.** Estrada A, Wright DL, Anderson AC. Antibacterial antifolates: from development through resistance to the next generation. Cold Spring Harbor perspectives in medicine. 2016; 6(8):a028324. https://doi.org/10.1101/cshperspect.a028324 PMID: 27352799

**86.** Sadaka C, Ellsworth E, Hansen PR, Ewin R, Damborg P, Watts JL. Review on abyssomicins: Inhibitors of the chorismate pathway and folate biosynthesis. Molecules. 2018; 23(6):1371. https://doi.org/10.3390/molecules23061371 PMID: 29882815

**87.** Frey KM, Viswanathan K, Wright DL, Anderson AC. Prospective screening of novel antibacterial inhibitors of dihydrofolate reductase for mutational resistance. Antimicrobial agents and chemotherapy. 2012; 56(7):3556–3562. https://doi.org/10.1128/AAC.06263-11 PMID: 22491688

**88.** Wróbel A, Drozdowska D. Recent design and structure-activity relationship studies on the modifications of DHFR inhibitors as anticancer agents. Current Medicinal Chemistry. 2021; 28(5):910–939. https://doi.org/10.2174/0929867326666191016151018 PMID: 31622199

**89.** Close SJ, McBurney CR, Garvin CG, Chen DC, Martin SJ. Trimethoprim-sulfamethoxazole activity and pharmacodynamics against glycopeptide-intermediate *Staphylococcus aureus*. Pharmacotherapy: The Journal of Human Pharmacology and Drug Therapy. 2002; 22(8):983–989. https://doi.org/10.1592/phco.22.12.983.33599 PMID: 12173801

**90.** Li J, Bi W, Dong G, Zhang Y, Wu Q, Dong T, et al. The new perspective of old antibiotic: in vitro antibacterial activity of TMP-SMZ against *Klebsiella pneumoniae*. Journal of Microbiology, Immunology and Infection. 2020; 53(5):757–765. https://doi.org/10.1016/j.jmii.2018.12.013 PMID: 30857922

**91.** Songsungthong W, Yongkiettrakul S, Bohan LE, Nicholson ES, Prasopporn S, Chaiyen P, et al. Diaminoquinazoline MMV675968 from Pathogen Box inhibits *Acinetobacter baumannii* growth through targeting of dihydrofolate reductase. Scientific Reports. 2019; 9(1):15625. https://doi.org/10.1038/s41598-019-52176-8 PMID: 31666629

**92.** Wu H, Chen H, Zhang J, Hu X, Xie C, Cao W, et al. The anti-multidrug-resistant *Acinetobacter baumannii* study on 1, 3-diamino-7H-pyrrolo [3, 2-f] quinazoline compounds. Molecules. 2022; 27(23):8609. https://doi.org/10.3390/molecules27238609 PMID: 36500701

**93.** Eisenberg RC, Dobrogosz WJ. Gluconate metabolism in *Escherichia coli*. Journal of Bacteriology. 1967; 93(3):941–949.

**94.** Britigan BE, Chai Y, Cohen M. Effects of human serum on the growth and metabolism of *Neisseria gonorrhoeae*: an alternative view of serum. Infection and immunity. 1985; 50(3):738–744.

**95.** Hommes R, Postma P, Tempest D, Neijssel O. The influence of the culture pH value on the direct glucose oxidative pathway in *Klebsiella pneumoniae* NCTC 418. Archives of microbiology. 1989; 151 (3):261–267. https://doi.org/10.1007/BF00413140 PMID: 2650650

**96.** Lessie T, Phibbs P Jr. Alternative pathways of carbohydrate utilization in pseudomonads. Annual review of microbiology. 1984; 38(1):359–388. https://doi.org/10.1146/annurev.mi.38.100184.002043 PMID: 6388497

**97.** Krismer B, Liebeke M, Janek D, Nega M, Rautenberg M, Hornig G, et al. Nutrient limitation governs *Staphylococcus aureus* metabolism and niche adaptation in the human nose. PLoS pathogens. 2014; 10(1):e1003862. https://doi.org/10.1371/journal.ppat.1003862 PMID: 24453967

**98.** Olivier BG, Bergmann FT. SBML level 3 package: flux balance constraints version 2. Journal of integrative bioinformatics. 2018; 15(1). https://doi.org/10.1515/jib-2017-0082 PMID: 29522419

**99.** Hastings J, Owen G, Dekker A, Ennis M, Kale N, Muthukrishnan V, et al. ChEBI in 2016: Improved services and an expanding collection of metabolites. Nucleic acids research. 2016; 44(D1):D1214–D1219. https://doi.org/10.1093/nar/gkv1031 PMID: 26467479

**100.** Karp PD, Billington R, Caspi R, Fulcher CA, Latendresse M, Kothari A, et al. The BioCyc collection of microbial genomes and metabolic pathways. Briefings in bioinformatics. 2019; 20(4):1085–1093. https://doi.org/10.1093/bib/bbx085 PMID: 29447345

**101.** Clark K, Karsch-Mizrachi I, Lipman DJ, Ostell J, Sayers EW. GenBank. Nucleic acids research. 2016; 44(D1):D67–D72. https://doi.org/10.1093/nar/gkv1276 PMID: 26590407

**102.** Chang A, Jeske L, Ulbrich S, Hofmann J, Koblitz J, Schomburg I, et al. BRENDA, the ELIXIR core data resource in 2021: new developments and updates. Nucleic Acids Research. 2021; 49(D1):D498–D508. https://doi.org/10.1093/nar/gkaa1025 PMID: 33211880

**103.** UniProt: the universal protein knowledgebase in 2021. Nucleic acids research. 2021; 49(D1):D480–D489. https://doi.org/10.1093/nar/gkaa1100 PMID: 33237286

**104.** Juty N, Le Novere N, Laibe C. Identifiers. org and MIRIAM Registry: community resources to provide persistent identification. Nucleic acids research. 2012; 40(D1):D580–D586. https://doi.org/10.1093/nar/gkr1097 PMID: 22140103

**105.** Römer M, Eichner J, Dräger A, Wrzodek C, Wrzodek F, Zell A. ZBIT bioinformatics toolbox: a web-platform for systems biology and expression data analysis. PloS one. 2016; 11(2):e0149263. https://doi.org/10.1371/journal.pone.0149263 PMID: 26882475

**106.** Courtot M, Juty N, Knüpfer C, Waltemath D, Zhukova A, Dräger A, et al. Controlled vocabularies and semantics in systems biology. Molecular systems biology. 2011; 7(1):543. https://doi.org/10.1038/msb.2011.77 PMID: 22027554

**107.** Altschul SF, Gish W, Miller W, Myers EW, Lipman DJ. Basic local alignment search tool. Journal of molecular biology. 1990; 215(3):403–410. Basic local alignment search tool. https://doi.org/10.1016/S0022-2836(05)80360-2 PMID: 2231712

**108.** Davis JJ, Wattam AR, Aziz RK, Brettin T, Butler R, Butler RM, et al. The PATRIC Bioinformatics Resource Center: expanding data and analysis capabilities. Nucleic acids research. 2020; 48(D1): D606–D612.

**109.** King ZA, Dräger A, Ebrahim A, Sonnenschein N, Lewis NE, Palsson BO. Escher: a web application for building, sharing, and embedding data-rich visualizations of biological pathways. PLoS computational biology. 2015; 11(8):e1004321. https://doi.org/10.1371/journal.pcbi.1004321 PMID: 26313928